

February 1995

PAR-LPTHE 9513, SU-HEP 4241-608, EFI 95-17

hep-th/9xmmmnn

Self-Avoiding Surfaces in the 3-d Ising Model

Vladimir S. Dotsenko*, Marco Picco and Paul Windey

LPTHE[†]

Université Pierre et Marie Curie - PARIS VI

Université Denis Diderot - Paris VII

Boite 126, Tour 16, 1^{er} étage

4 place Jussieu

F-75252 Paris CEDEX 05, FRANCE

Geoffrey Harris[‡]

Physics Department, Syracuse University

Syracuse, NY 13244, USA

Emil Martinec

Enrico Fermi Institute and Department of Physics,

University of Chicago

Chicago, IL 60637, USA

Enzo Marinari

Dipartimento di Fisica and INFN

Università di Cagliari,

Via Ospedale 72, 09100 Cagliari, ITALY

*Also at the Landau Institute for Theoretical Physics, Moscow

[†]Laboratoire associé No. 280 au CNRS

[‡]present address: Enrico Fermi Institute and Department of Physics, University of Chicago

ABSTRACT

We examine the geometrical and topological properties of surfaces surrounding clusters in the 3- d Ising model. For geometrical clusters at the percolation temperature and Fortuin–Kasteleyn clusters at T_c , the number of surfaces of genus g and area A behaves as $A^{x(g)}e^{-\mu(g)A}$, with x approximately linear in g and μ constant. These scaling laws are the same as those we obtain for simulations of 3- d bond percolation. We observe that cross-sections of spin domain boundaries at T_c decompose into a distribution $N(l)$ of loops of length l that scales as $l^{-\tau}$ with $\tau \sim 2.2$. We also present some new numerical results for 2- d self-avoiding loops that we compare with analytic predictions. We address the prospects for a string-theoretic description of cluster boundaries.

1 Introduction

One of the major successes of 20th century physics has been the expression of the critical behavior of a variety of theories of nature in terms of sums over decorated, fluctuating paths. It has thus been hoped that higher dimensional analogues, theories of fluctuating membranes, also play a fundamental role in characterizing the physics of critical phenomena. In particular, significant effort has been invested in recasting one of the simpler models of phase transitions, the $3-d$ Ising model, as a theory of strings [1]. These attempts have been stymied by the difficulty in taking the continuum limit of formal sums over lattice surfaces.

In fact, sums over lattice surfaces, built from e.g. plaquettes or polygons, generically fail to lead to a well-defined continuum theory of surfaces. An exception to this rule occurs when the surface discretizations are embedded in $d \leq 1$. In this case, one can exactly solve a large class of toy lattice models which lead to sensible continuum ‘bosonic’ string theories (at least perturbatively) [2]. Numerically, it is observed that the $d > 1$ versions of these lattice models suffer a ‘fingering instability’; the embedded surfaces, for instance are composed of spikes with thickness of the order of the cutoff. It is suspected that the polygonal discretization of the worldsheet (for large volumes) is configured in a polymer-like structure, so that these theories cannot be realized as sums over surfaces in the continuum limit. This instability is anticipated theoretically, since the mass-squared of the dressed identity operator of the bosonic string becomes negative above $d = 1$, presumably generating a uncontrolled cascade of states that tear the worldsheet apart[3].

In the continuum limit, we know how to evade these problems in special cases through the implementation of supersymmetry and the GSO projection. This additional structure, however, leads to fundamental difficulties in discretizing these theories. In principle, one might hope to somehow guess an appropriate continuum string theory and then show that it embodies the critical behavior of a lattice theory, such as the $3-d$ Ising model. The prospects for success through such an approach seem rather poor at this time.

Given this state of affairs, we have turned to a more phenomenological approach, in which we attempt to generate ‘physical’ random surfaces in a particular model and then examine

their topological and geometrical properties. We thus have chosen to look at the structure of domain boundaries in the 3- d Ising model. The phenomenology of these self-avoiding cluster boundaries is interesting in its own right, since it describes a large universality class of behavior that is expressed frequently and quite precisely by nature. We also might hope that our observations may be useful in gauging the prospects of success of a string-theoretic description. The Ising model has been employed previously as a means to generate random lattice surfaces ¹; see for instance, the work of David [4], Huse and Leibler [5], Karowski and Thun and Schrader [6]. In a sense, this work extends these studies by looking for new features of the geometry of these lattice surfaces; we also consider boundaries of Fortuin–Kasteleyn clusters as well as ‘geometrical’ spin domains. Much of our analysis consists of a measurement of the distribution of surfaces as a function of their area A and genus g , $N_g(A)$ ². We shall determine the functional form of $N_g(A)$. We also perform block spin measurements of the genus, to determine if a condensation of handles is present on cluster boundaries at all scales. These cluster boundaries are strongly coupled and thus it appears cannot be directly characterized by perturbative string theory. We see that, however, boundaries of spin domains at the Curie temperature are not just strongly-coupled versions of the branched polymer-like objects that attempts to build ‘bosonic’ random surfaces typically generate. They instead exhibit a richer fractal structure, albeit one not characteristic of surfaces. We show that they obey a new scaling law that describes the distribution $N(l)$ of lengths l of loops that compose cross-sections of cluster boundaries.

In the course of these investigations, we generated a considerable amount of data characterizing additional geometric properties of Ising clusters and their bounding surfaces. In particular, we also simulated the two-dimensional Ising model. In the two-dimensional case, there exist many exact results describing the fractal structure and distribution of clusters and loops. To provide a more comprehensive and complete picture of the geometry of Ising surfaces, we shall present these additional results in this paper. In some cases, these addi-

¹Through the use the phrase ‘lattice surface’ rather than ‘surface’, we indicate that these objects should *not* be necessarily inferred to be real surfaces in the continuum limit.

²The mean genus per Ising configuration is measured in references [6]. A determination of genus as a function of area in an Ising system with anti-periodic boundary conditions has been made [7].

tional results have been verified previously, though generally on smaller lattices and with somewhat less numerical precision.

2 Ising Clusters and Surfaces

We shall begin by summarizing the basic physical properties of the cluster boundaries that we have analyzed. To a first approximation, a 2-dimensional membrane of area A and curvature matrix K will exact an energy cost [5, 8]

$$H = \mu A + \lambda \int (\text{Tr}K)^2 + \kappa \int \text{Det}K; \quad (2.1)$$

μ is the bare surface tension, λ is referred to as the bending rigidity and κ couples to the Euler character of the surface. In the regime which characterizes random surfaces, the surface tension must be sufficiently small to allow significant thermal fluctuations. Note that the above action does not constitute a complete physical description of the Ising surfaces. It is essential also to keep in mind the constraint that Ising cluster boundaries are naturally self-avoiding. We first consider surfaces in the dual lattice that bound ‘geometrical clusters’ formed from sets of adjacent identical spins. In this case, the Ising dynamics generates an energy penalty proportional to the boundary area; λ_{bare} and $\kappa_{bare} = 0$. The bare surface tension is tuned by the Ising temperature. To put this model in perspective, we note that for real vesicles, for instance, the couplings λ and κ can be quite large; λ ranging from about kT to $100kT$ have been measured [8]. The bending rigidity may be irrelevant in the continuum limit, however. The string coupling³ is equal to $\exp(-\kappa)$. Through blocking spins, we make an estimate of the renormalization group behavior of κ . Unless κ effectively becomes large in the infrared, the cluster boundaries will fail to admit a surface description in the continuum limit.

The geometrical clusters and their boundaries are *not* present at all scales at the Curie temperature. Instead, for temperatures somewhat below T_c and all temperatures above T_c two huge geometrical clusters comprise a finite fraction of the entire lattice volume. These

³We ignore distinctions between intrinsic and extrinsic metrics.

clusters percolate, that is, they wrap around the entire lattice (we shall consider periodic boundary conditions). Otherwise, the lattice only contains very small clusters that are the size of a few lattice spacings; there are no intermediate size clusters. We can understand this behavior by considering the $T \rightarrow \infty$ behavior of these clusters. Two percolated clusters span the lattice even at infinite temperature, where clusters are smaller than at T_c . At $T = \infty$, the spins are distributed randomly with spin up with probability 50%; the problem of constructing clusters from these spins then reduces to pure site percolation with $p = 1/2$. Pure site (or bond) percolation describes the properties of clusters built by identifying adjacent colored bonds (sites), which are colored randomly with probability p . Above a critical value $p = p_c$, the largest of these clusters percolates through the lattice[9]. For the cubic lattice, it is known that an infinite cluster will be generated (in the thermodynamic limit) at $p_c \sim .311$. Thus, the fact that the geometrical clusters have percolated in the high-temperature regime and at the Curie point is essentially a consequence of the connectivity of 3- d lattices.

At very low temperatures, however, there are few reversed (minority) spins in the Ising model; these form a few small clusters. As the density of minority spins increases, the clusters become bigger until the largest cluster percolates at some temperature $T_p < T_c$. It has been suggested (see [10] and [5]) that since this minority spin percolation appears to be due to an increase in the concentration of minority spins and not to any long-distance Ising dynamics, that this transition is in the same universality class as pure (bond or site) percolation. We emphasize that the scaling of minority clusters should not correspond to any non-analyticity in the thermodynamic behavior of the Ising model; it should essentially be a ‘geometric effect’.

There is another type of cluster, introduced by Fortuin and Kasteleyn [11, 12], that does proliferate over all length scales at the Curie point. These FK clusters consist of sets of bonded spins; one draws these bonds between adjacent same-sign spins with a temperature dependent probability $p = 1 - \exp(-2\beta)$. Note that the geometrical clusters are built by a similar procedure, using instead $p = 1$. FK clusters arise naturally in the reformulation of the Ising model as a percolating bond/spin model [13]. For the Ising partition function can

be rewritten as a sum over occupied and unoccupied bonds with partition function

$$Z = \sum_{\text{bonds}} p^b (1-p)^{(N_b-b)} 2^{N_c} \quad (2.2)$$

where $p = 1 - \exp(-2\beta)$, N_b denotes the number of bonds in the entire lattice in which b bonds are occupied and N_c equals the number of clusters that these occupied bonds form. When the factor 2^{N_c} is replaced by q^{N_c} , then (2.2) is the partition function for the q -state Potts model. If we assign a spin to each bond so that all bonds in the same cluster have the same spin, then the factor of q^{N_c} just comes from a sum over spin states. The above partition function can then be viewed as a sum over FK clusters. Using this construction, one can show that the spin-spin correlator in the original Ising model is equal to the pair connectedness function of FK clusters,

$$\langle \sigma(x)\sigma(y) \rangle = \langle \delta_{C_x, C_y} \rangle, \quad (2.3)$$

which equals the probability that points x and y belong to the same FK cluster [14]. It then follows that for $T \geq T_c$, the mean volume of the FK clusters is proportional to the susceptibility of the Ising model, so that indeed FK clusters only just start to percolate at the Curie point. Additionally, the relation (2.3) also implies that the spatial extent of the FK clusters is proportional to the correlation length of the Ising model. Furthermore, scaling arguments [15] demonstrate that at T_c , the volume distribution of FK clusters obeys

$$N(V) \simeq V^{-\tau}, \quad \tau = 2 + \frac{1}{\delta}, \quad (2.4)$$

where δ denotes the magnetic exponent of the Ising model ($M \simeq B^{1/\delta}$). Thus we see that FK clusters, unlike the geometrical clusters previously discussed, directly encode the critical properties of the Ising model. Indeed, we are necessarily led to study FK clusters in order to measure scaling laws that characterize cluster boundaries of the scale of the Ising correlation length, i.e. boundaries that scale at the Curie point. On the other hand, geometrical cluster boundaries contribute an energy penalty proportional to their individual area; the lattice surface dynamics of FK cluster boundaries, however, cannot be likewise described by a similar physical rule.

In 2-dimensions both the FK clusters and the geometrical clusters percolate at the Curie temperature. The critical properties of these clusters differ, however, since the scaling of

geometrical clusters is partially determined by the ‘percolative’ properties of two-dimensional lattices. These effects are in some sense removed through the FK construction. We will present below numerical results for $2-d$ geometrical clusters, which can be compared with theoretical predictions[16, 17].

3 The Simulation

We now proceed to outline the techniques used in our Monte Carlo simulations. We performed a set of medium-sized simulations using about one year of time on RISC workstations. We collected data on a variety of two and three-dimensional lattices: square, triangular, simple cubic and BCC (see below). A third set of measurements of distributions of loop sizes was made on two-dimensional slices of three-dimensional lattices. A summary of the size of our runs appears in tables 1-3.

Spin updates were implemented through the efficient Swendsen–Wang algorithm [18]: FK clusters for each lattice configuration are first constructed, then the spins composing each cluster are (all) assigned a new random spin value.

The main technical difficulty that we encountered (in three dimensions) was the measurement of the Euler character, equal to $V - E + F$ for a dual surface with V vertices, E edges and F faces. On the simple cubic (SC) lattice, the construction of the dual surface and measurement of genus is ambiguous. Each surface is built from plaquettes composing the phase boundary between a pair of clusters, e.g. cluster a and cluster b . One can then associate with this surface the set of cubes in the dual lattice that surround sites in cluster a along the surface boundary. To measure genus we must then resolve two types of ambiguities in building these surfaces. These ambiguities occur when the associated cubes intersect along just one link or intersect only at a vertex. One has to decide, for example, whether to connect cubes that touch at just a vertex with a thin tube or to instead, split them, so they no longer touch. We came up with three separate algorithms (two of which turned out to be equivalent) that are consistent in the following sense: they yield the standard value of genus when no ambiguities were present and they always lead to a genus that is a

non-negative integer. We chose, for instance, to split cubes that touched at just one point. A consistent algorithm to measure genus on the simple cubic lattice is also presented in the work of Caselle, Gliozzi and Vinti[7].

Since these rules are not unique, one would hope that their implementation essentially serves as a regularization that does not affect long-distance scaling laws. In fact, in order to eliminate any doubts about our rules, we also performed simulations on specially chosen lattices where ambiguities are absent. In two dimensions, one can avoid ambiguous intersections on the dual lattice by considering Ising spins on the triangular lattice. Its dual (the honeycomb lattice) is trivalent and thus Ising spin domains will not be enclosed by self-intersecting paths. This fortuitous situation generalizes to three-dimensions for the Ising model on a body centered cubic (BCC) lattice in which the vertices at the center of each cube are also connected to those in the centers of neighboring cubes. More explicitly, we coupled with equal strength both the 6 nearest and 8 next-nearest Ising spins so that only three plaquettes of the dual lattice meet along a dual link. Since surfaces built dual to this lattice are also naturally self-avoiding, computing the genus is trivial. A depiction of the Wigner-Seitz cell of this lattice (composed of plaquettes in the dual lattice) appears in figure 3.1.

In two dimensions, measurements were performed at the Curie temperature. Configurations of FK clusters and cross-sectional slices were taken at the three-dimensional Curie temperature. For the SC lattice, this value is well known [20]. On the BCC lattice with second nearest neighbor interactions, we determined the Curie temperature by adjusting β until we found optimal scaling for the cluster size distribution. In three dimensions, we examined the scaling of geometrical clusters at the percolation temperature β_P . We determined this using a method discussed by Kirkpatrick [21] in which one measures the fraction of configurations f containing clusters that span the lattice as a function of β . One plots f versus β for different lattice sizes L ; β_P corresponds to the intersection of these curves for different L .

Statistical errors are computed using binning and the jackknife technique. We determine exponents through linear least-squared fits; statistical errors for these exponents are also

obtained by using jackknife when fitting. Generally, systematic errors swamp our statistical errors. These systematic effects are due to finite-size effects, the failure to reach the asymptotic scaling region as well as the uncertainty in the value of the critical temperature in certain cases. The absence of a quoted error or an errorbar henceforth indicates that the statistical error is much smaller than our measured observable or that the errorbars are too small to appear on our plots. In particular cases (when we examine slices of 150^3 lattices), our data will not be sufficient to accurately estimate the jackknife error. We are confident in these cases, though, that the statistical error is still much smaller than the systematic error.

4 Clusters and self-avoiding loops in the 2D Ising model

In order to check our methods and techniques we first turn to the $2-d$ Ising model. In fact, in two dimensions, a large number of critical exponents have been computed by using conformal field theory techniques [16, 17]. We shall see that our measurements agree with these predictions. We determined the scaling properties of geometrical clusters and of self-avoiding loops bounding these clusters on square and triangular lattices with sizes up to 1000×1000 . The measured scaling laws and lattices were chosen for their similarity to the three dimensional analogues that we are most interested in. In particular, the honeycomb lattice (dual to the triangular lattice) is well known to produce self-avoiding loops in a natural way since it has a coordination number equal to three. It is analogous in this respect to the dual of the BCC lattice in three dimensions. For both the triangular lattice and the BCC lattice, there exists no ambiguities in defining the boundary of a spin cluster.

The equilibrium configurations were produced by a Swendsen–Wang cluster algorithm at $T_c = 0.44068\dots$ for the square lattice, and at $T_c = 0.27465\dots$ for the triangular lattice. This algorithm is supposed to have a relaxation time exponent equal to zero precisely for the $2-d$ Ising model [19]. After every 10 cluster updating steps we analyzed the resulting spin configuration. For each of these configurations we measured $N(l)$, the statistical distribution of the self-avoiding loops bounding the spin clusters, as a function of the length of their perimeter. We also measured $A(l)$, the average total area inside these loops.

The definition of what we call $A(l)$ needs to be made precise: by area $A(l)$ we mean the *total* area enclosed by a given loop of length l . This area includes the spin cluster bounded by the loop of length l ; it also incorporates all of the islands of flipped spins imbedded within this cluster. We consider all loops, not just the outer ones and each given loop is considered as an outer boundary or “hull” of the complete figure inside. We used this definition since it appears to be the most natural for the problem of self-avoiding loops. It makes sense to consider all loops, since on an infinite lattice, any given loop would be inside other larger loops at T_c .

We define the exponents τ and δ by

$$N(l) \simeq l^{-\tau} \tag{4.1}$$

and

$$A(l) \simeq l^\delta. \tag{4.2}$$

The values that we obtained for τ and δ are listed in tables 4 and 5. The windows (intervals of l) were chosen as usual to minimize the influence of corrections to scaling at small l and finite-size effects at large l . The errors that we quote for these exponents reflect the systematic uncertainty arising from our choice of windows. These systematic errors should be larger than the statistical uncertainties, which nonetheless are difficult to estimate.

Our best results were obtained with the 1000×1000 triangular lattice. They give the following scaling exponents for self-avoiding loops in two dimensions:

$$\tau = 2.44 \pm 0.01, \quad \delta = 1.454 \pm 0.002. \tag{4.3}$$

The remarkable scaling behavior of $N(l)$ and $A(l)$ is displayed (in log – log plots) respectively in figure 4.1 and figure 4.2.

The values of the exponents in (4.3) can be compared with the theoretical predictions based on the Coulomb gas representation [16] and with further scaling arguments originally due to B. Duplantier [22]⁴. This theoretical analysis yields the scaling relation:

$$\tau = 1 + \delta \tag{4.4}$$

⁴For an alternate derivation of a similar relation in the case of percolation theory, see section 3.4 of Stauffer’s book[9]

with a value for δ of

$$\delta = \frac{2}{D_H} = \frac{16}{11} = 1.4545\dots \quad (4.5)$$

Here $D_H = \frac{11}{8}$ [16] is the fractal dimension commonly used for the cluster “hulls”. One observes that our numerical values (4.3) are in good agreement with these theoretical predictions. We shall present a version of Duplantier’s derivation of the relation between τ and δ in the appendix.

Previous numerical work on other exponents related to D_H can be found in [23, 24]. The results of these papers support the theoretical value of D_H given above. One should remark that our simulations, which are done on a much larger lattice (1000^2 rather than 36^2 as in [24]), yield much more accurate values of the exponents.

Finally, we measured on the triangular lattice the universal ratio

$$\frac{A(l)}{R^2(l)} = r_l. \quad (4.6)$$

r_l , which was recently computed by Cardy [17], is the ratio of the area inside a loop of length l to the squared radius of gyration of this same loop, defined by

$$R^2 = \frac{1}{2l^2} \sum_{r_1, r_2} (r_1 - r_2)^2 \quad (4.7)$$

(r_1, r_2 are the positions of the links of the loop on the lattice). The result obtained by Cardy is

$$r_l \sim \frac{1 + 2g}{2(1 + 2g)}\pi \quad (4.8)$$

where g is a Coulomb gas parameter with $g = \frac{4}{3}$ for Ising clusters at T_c and $g = \frac{2}{3}$ for Ising clusters at $T = \infty$ (which in fact corresponds to the pure percolation point on the triangular lattice; this point is discussed in section 5.3). The values that we obtained for r_l^c (r_l at the critical temperature) and r_l^∞ (r_l at $T = \infty$) are listed in table 6. Here again, intervals were chosen so as to avoid lattice artifacts at small l and finite-size effects at large l . From our measurements, we deduce, for the 1000×1000 lattice, the following value at the critical temperature:

$$r_l^c = 2.471 \pm 0.001; \quad (4.9)$$

the exact value given by Cardy is $r_l^c = \frac{11}{14}\pi \simeq 2.468\dots$. The measured quantity again approaches the exact value as we increase the lattice size. On 500×500 lattices, the measured value is $r_l^c = 2.472 \pm 0.001$ while on 250×250 lattices, which we also simulated, it is $r_l^c = 2.478 \pm 0.002$.

For the percolation case (*i.e.* $T = \infty$), the value given by Cardy is $r_l^\infty = \frac{7}{10}\pi \simeq 2.199\dots$. We obtain, for the 1000×1000 lattice, the value

$$r_l^\infty = 2.218 \pm 0.001. \quad (4.10)$$

This differs from Cardy's prediction by about 1 percent. But again, as we increase the lattice size, the measured value approaches the exact value. For the percolation case, lattice artifacts at small l are important up to a value of l of order $\simeq 200$. We are able to obtain only limited statistics in the regime that exhibits good asymptotic behavior.

5 Results for 3D Clusters

We now present data from our simulations on both the simple cubic and BCC lattices. We have examined boundaries of FK clusters at T_c , surfaces bounding minority spin domains at T_p , geometrical clusters at T_c and pure bond percolation. A more concise summary of some of these results has been presented in [25, 26].

5.1 Cluster Geometry

We begin by discussing geometrical properties of the clusters. Some of the material in this section is already well known, but we present it to illustrate the influence of lattice artifacts and finite-size effects in our data. This analysis will allow us to determine the range of parameters for which we will be able to best trust our results.

First, we shall analyze the data for FK clusters on the simple cubic lattice with volumes 32^3 and 64^3 . We fit to the cluster distribution function

$$N(V) \simeq V^{-\tau}, \quad (5.1)$$

where V is the cluster volume in real space (see figure 5.1).

As a first check we have reproduced the exact fit used by Wang in ref. [15], by using volumes ranging from 4 to 64. Wang quotes here a value of 2.30 (against the expected value of 2.21⁵).

Our best fits for V ranging from 4 to 64 (which we present here only for the sake of comparison) give $\tau_{L=32}^{FK} = 2.310$, $\tau_{L=64}^{FK} = 2.299$, where in both cases the statistical error is less than one in the last digit. Note that τ^{FK} decreases slightly as a function of increasing lattice size. It is evident that the lattice sizes we used are not sufficient to exclude both significant corrections to scaling (for small V) or finite-size effects (afflicting $V \sim L^3$). We do not observe a convincing plateau in plots of $\log N(V)$ vs. $\log V$. The closest the data comes to plateauing on $L = 32$ lattices is in the volume range $V \in (32, 1024)$, where we extract $\tau_{L=32}^{FK} = 2.324 \pm .001$. We obtain $\tau_{L=64}^{FK} = 2.286 \pm .001$ on $L = 64$ lattices.

Likewise, on the *BCC* lattice, we see large deviations from power-law scaling of $N(V)$. In this case, our values of τ_{FK} are quite close to the theoretical prediction of 2.21; for $L = 64$ we measure $\tau^{FK} = 2.235$ and 2.218 on the volume windows (32, 1024) and (64, 1024) respectively. This agreement with theory should be viewed with a great deal of caution, given the large systematic effects that are present.

Similar results hold in the analysis of $N(V)$ for geometrical clusters at T_p . Significant deviations from scaling are again present. We measure smaller values of τ than in the FK case: $\tau_{L=30}^{GC} = 2.069 \pm .005$, $\tau_{L=60}^{GC} = 2.124 \pm .002$ and $\tau_{L=100}^{GC} = 2.13 \pm .002$ on windows of size (32, 256), (64, 2048) and (64, 4096) respectively. One would anticipate that the value of τ for geometrical clusters would be characteristic of the scaling of pure percolation clusters. For pure bond percolation, the scaling exponents have been determined primarily through series expansions and to a lesser extent through Monte Carlo techniques; these analyses give a value of τ that is centered about 2.18 with an uncertainty of roughly 0.02 [9].

We also measure $N(V)$ explicitly for 3d bond percolation; in this case, the data are much cleaner. On the 32 to 1024 window, for example, we get an exponent of 2.217 ± 0.001 both on

⁵In particular, by applying the scaling relations to the results of ϵ expansions, one expects $\tau = 2.207(1)$ [27], high temperature expansions yield $\tau = 2.210(1)$ [28] and RG calculations give $\tau = 2.207(< 1)$ [29].

the 32^3 and 64^3 lattice. On the 128-2048 window we see the first (small!) signs of finite size effects, with a value of 2.200 ± 0.004 for the small lattice and 2.209 ± 0.002 on the large lattice. The results are so precise and consistent in this case that we can attempt a fit to finite size corrections; this yields a result in between 2.18 and 2.21, in complete agreement with the numbers cited in the literature [9]. We stress that this extrapolated number apparently has a much smaller systematic error than the ones we have quoted in other cases.

It is thus evident that the power law fits to $N(V)$ are a rather poor way to measure critical exponents; much more accurate estimates can be obtained through finite-size scaling fits of the mean cluster size as a function of lattice size L . We now present our finite-size scaling analysis. First, we have measured the scaling behavior (from $L = 32$ to $L = 64$) for the mean cluster size

$$\frac{\langle V^2 \rangle}{\langle V \rangle} \simeq L^{\mathcal{H}}, \quad (5.2)$$

finding an exponent of 1.97 ± 0.01 for FK Ising clusters on the SC lattice, an exponent of 1.99 ± 0.01 for geometrical clusters on the BCC lattice (where we extrapolate from $L = 30$ to $L = 100$), and an exponent of 2.09 ± 0.01 for bond percolation ⁶. Since the mean cluster size is proportional to the susceptibility, it obeys the finite-size scaling relation characteristic of the susceptibility at β_c , so $\mathcal{H} = \frac{\gamma}{\nu}$. For the $3d$ Ising model, predictions for $\frac{\gamma}{\nu}$ are 1.97(1), 1.95(1) and 1.97(1) from ϵ expansions, high temperature series and renormalization group calculations respectively. Series expansions, Monte Carlo simulations and ϵ expansions have been also applied to the calculation of pure percolation exponents. In this case, they have yielded the values $\frac{\gamma}{\nu} = 2.07(16), 2.05(2)$ and $2.19(11)$ respectively. Our measurements of the finite-size scaling behavior of the mean cluster size thus appear to yield precise and correct estimates of $\frac{\gamma}{\nu}$. Now, using some standard scaling relations and (2.4) it is also possible to relate $\frac{\gamma}{\nu}$ to τ and then obtain a second measurement of τ :

$$\tau = (3 + \gamma/\nu d)/(1 + \gamma/\nu d) \quad (d = 3) \quad (5.3)$$

⁶ Note that we ran our bond percolation simulations at $p = .249$; recent Monte Carlo work indicates that actually p_c may be as low as .2488 [30] in this case. We would then estimate (by noting how sensitive \mathcal{H} is to p) that the uncertainty in p_c contributes to a systematic error of roughly 0.02 – 0.03 in \mathcal{H} for percolation. Since the Curie temperature is known much more precisely, this bias is not significant for FK clusters.

Using this technique, we measured $\tau_{\text{FK}} = 2.207(3)$ on the SC lattice and $\tau_{\text{geo}} = 2.202(3)$ on the BCC lattice. The error on τ_{geo} is in fact probably several times larger than quoted above, due to uncertainties in locating the critical temperature. This measurement of τ_{FK} agrees perfectly with previous values; the measurement of τ_{geo} is not accurate enough to distinguish likely pure percolation behavior from that of percolation of FK clusters.

We have also measured the exponent given by the scaling of the maximal cluster volume, defined by

$$\langle V_{Max} \rangle \simeq L^{\mathcal{J}} , \quad (5.4)$$

finding 2.49 ± 0.01 for SC FK Ising clusters, 2.53 ± 0.01 for BCC geometrical clusters and 2.56 ± 0.01 for bond percolation. One can show via scaling arguments (from the relation (5.1)) that $\mathcal{J} = \frac{3}{\tau-1}$ and then applying standard scaling relations, that $\mathcal{H} = 2\mathcal{J} - 3$. We thus see that our values of \mathcal{J} are consistent with those of \mathcal{H} .

To get a better picture of the cluster geometry, we also examined the dependence of the cluster surface extent A_c on its volume V . Note that for $V < 6$, the simple cubic lattice structure demands $V = A_c$. For slightly higher volumes, clusters do begin to form interior points, so that A_c becomes less than V .

It is well known that typical pure percolation clusters are saturated with holes and crevasses which break up their scant interiors. Since unoccupied bonds are distributed homogeneously with probability $1 - p$, there is a fixed probability per unit area that any site will not be pierced by occupied bonds, but that its neighboring site will belong to a cluster. From this argument one can deduce [31] that the cluster perimeter (defined as the number of empty sites adjacent to an occupied cluster site) is linearly proportional to the cluster volume; percolation clusters are tubular and very branched.

Note that FK clusters are formed by implementing pure bond percolation on geometrical Ising clusters. Therefore, one might anticipate that they at least qualitatively might share some of the geometrical characteristics of pure percolation clusters. In particular, one could argue that their perimeter should be linearly proportional to their volume by applying the above reasoning. Indeed, in all cases (FK, geometrical and pure percolation clusters), we found that the cluster perimeter was proportional to the enclosed volume. This dependence

can be characterized by the effective exponent ω , given by

$$A_c \sim V^\omega . \tag{5.5}$$

For instance, we find that on the 64^3 lattice, in the window $49 < V < 293$, $\omega^{FK} = 0.980$; ω steadily grows as V increases until it reaches 0.992(1) in the window $611 < V < 841$.

5.2 Cluster Topology

We have computed the quantity $N_g(A)$ (the number of dual surfaces of given genus g and area A) for the models that we have studied. Our data clearly show that we can model scaling laws for such complex quantities. It turns out that in all cases our data are described asymptotically by

$$N_g(A) = C_g A^{x(g)} e^{-\mu(g)A} , \tag{5.6}$$

we will discuss the cases in which, due to lattice artifacts and finite size effects, this behavior is not perfect. We have used in this formula a generic genus g dependence $x(g)$ and $\mu(g)$, but we will argue that our data suggests that asymptotically μ does not vary with genus and that $x(g)$ depends linearly on genus.

Indeed, one might anticipate a distribution of the form (5.6) if the handles are uncorrelated. In this case, we would posit that handles would sprout randomly from the surface with probability μ per unit plaquette. This would generate the above distribution, with $C_g \propto \mu^g/g!$, $x(g) = g$ and $\mu(g)$ independent of g . We shall refer to this behavior as the Poisson scenario. Much of the forthcoming analysis is devoted to a determination of whether this scenario holds.

We start by presenting typical plots of $N_g(A)$ along with best fits to the form (5.6) to give a sense of the quality of our results.

In figure 5.2 we show the behavior of genus 1 surfaces for the SC FK Ising clusters. Here the fit does not work. Near the maximum, the numerical data grows far more than the best fit allows. Genus 1 data on the SC lattice come indeed from fairly small surfaces (of order 100 plaquettes, corresponding to clusters of size of tens of sites) and a biased behavior is expected.

The situation is very different already for genus 5 as we show in figure 5.3. Here the scale is given by dual surfaces of the order of 500 plaquettes, encompassing clusters with of order one to two hundred sites, and a behavior closer to the continuum expectation is in order. The fit for figure 5.3 is indeed quite good, though some small systematic discrepancies survive, albeit more weakly, for larger genus, where the statistical error does eventually become very large. On the SC lattice we find indeed, both for the Ising model and for bond percolation, that our fits systematically overestimate $N_g(A)$ for small A and that near the peak they are slightly too low. Though this effect is very small already at genus 5 it is undoubtedly there. We recall here that our definition of genus on the SC lattice entails a resolution of short-distance ambiguities; perhaps this yields a regularization that affects the geometry of moderately large (though presumably not continuum) surfaces. Still, the SC fits are quite good.

We also present the fit for genus 5 surfaces bounding pure bond percolation clusters on the SC lattice (figure 5.4). The results resemble those for FK clusters; they are quite good apart from the deviations at the peak observed previously.

The most impressive data come from measurements of Ising FK clusters on the BCC lattice, for which there are no genus ambiguities. Here already the genus 2 data have an unbelievably clean behavior (see figure 5.5). $N_2(A)$ is peaked close to surfaces with order 250 plaquettes, and the fit is perfect apart from the very very small area region, where we do not expect scaling anyway. The functional form precisely describes both behavior for areas far below the maximum and near the maximum itself. Likewise, the power law plus exponential form captures all of the relevant features of the genus 5 data; this fit peaks at around 750 plaquettes (see figure 5.6). The fits continue to be superb for higher genus, though our statistics become too poor when we reach genus 15-20 to allow us to fit to the data directly and convincingly⁷. We also repeated these fits excluding data from surfaces of small area (less than 100, 150, 200, 250, ..., 650 plaquettes). Excluding these small areas makes essentially no difference in the resulting fits for $g \geq 3$.

⁷Note that errors on these (and all) plots are extremely correlated; this explains why it is possible for our best fit to pass dead-center through so many error bars.

For Ising geometrical clusters on the BCC lattice, the situation is not quite so good, at least for small genus. Indeed, for genus 2 data (see figure 5.7) there are large deviations from the best fit curve; near the maximum, the fit is too low, for example. The situation improves when we consider higher genus data. Genus 5 data (see figure 5.8) agree well with formula (5.6). In fact, for genus larger than 4, the fits of (5.6) to the data are nearly as good as the FK fits on the BCC lattice.

In conclusion, our ansatz of equation (5.6) is well satisfied in the scaling limit; we will proceed now to an analysis of the behavior of $x(g)$ and $\mu(g)$.

Let us start with $\mu(g)$ which, taking our cue from the behavior of two-dimensional quantum gravity[33], we refer to as the cosmological constant. In order to analyze our data we have used both the linear fits we have described above and we have also computed directly the moments of the area distribution. For data satisfying (5.6), the cosmological constant obeys

$$\mu = \mu_{eff} \equiv \frac{\langle A \rangle}{(\langle A^2 \rangle - \langle A \rangle^2)} \quad (5.7)$$

and the exponent $x(g)$ is given by

$$x(g) = x_{eff} \equiv \frac{\langle A \rangle^2}{(\langle A^2 \rangle - \langle A \rangle^2)} - 1 . \quad (5.8)$$

Additionally, the mean area then satisfies

$$\langle A \rangle = \frac{x_{eff} + 1}{\mu_{eff}} . \quad (5.9)$$

In the figure 5.9, we show the dependence on μ_{eff} for FK clusters on the 64^3 BCC lattice. The values of the cosmological constant obtained from our fits to (5.6) are equal (within a high degree of precision) to those obtained from the moments for $g \geq 3$. Clearly, the figure shows that the cosmological constant plateaus to a constant (0.0088 ± 0.0002), where the error is mainly due to systematic, not statistical, effects. This is one of the primary results that we present: the Ising model BCC FK data scale with a cosmological constant which does not depend on genus and is definitely not zero.

Figure 5.10 shows the dependence of μ_{eff} on g for geometrical clusters on the 60^3 BCC lattice. Here again there is clearly a plateau for the cosmological constant when $g \geq 10$ with

a value of 0.0033 ± 0.0002 . We also notice that for small genus (up to genus 10) the transient behavior of $\mu_{eff}(g)$ is significant; this reflects deviations in the best fits of $N_g(A)$ from the data.

Note that the value of μ essentially corresponds to the density of handles as a function of surface area. We find then on average that the area needed to grow a handle is of order 110 plaquettes on the BCC lattice for FK clusters and 300 plaquettes for geometrical clusters.

Next, we plot $x(g)$ (determined directly from fits) and x_{eff} (from moments) for FK clusters in the 64^3 BCC lattice (figure 5.11). Note that these quantities are indeed essentially identical for $g \geq 3$, substantiating the quality of our global fits. To see if $x(g)$ depends linearly on g , we also plot the difference $x(g) - x(g - 1)$ (see figure 5.12). This difference indeed roughly appears to plateau to a constant value, but given our statistics we cannot claim this to a great degree of precision. Additionally, we expect at some point that finite-size effects will also cause deviations from linearity. From the plateau, we would estimate the slope of $x(g)$ vs. g to be $1.25 \pm .10$, where the quoted error is due mainly to systematic effects.

In figure 5.13, we plot $x(g)$ (determined directly from fits) and x_{eff} (from moments) for geometrical clusters on the 60^3 BCC lattice. Here again these two quantities do not differ much when $g \geq 3$. Each of these plots looks like a linear function of g . Figure 5.14 shows $x_{eff}(g+1) - x_{eff}(g)$. Again, this shows a plateau to a value constant up to large fluctuations. In that case, the slope of $x(g)$ vs. g is 0.7 ± 0.1 .

The dependence of the mean area on genus can be measured much more accurately (since it does not depend on a fit or on a dispersion of moments). For FK clusters, we see from a plot of $\ln(\langle A \rangle)$ vs. $\ln(g)$ in the small genus regime that $\langle A \rangle$ is not precisely linear in g (see figure 5.15); in fact it scales roughly as $g^{.85}$. Note that such a scaling law could not hold asymptotically for large lattices and large areas, since it would imply that surfaces could have more handles than plaquettes. Indeed this effective exponent slowly increases with genus (to roughly .90 at $g = 50$). Thus we observe systematic deviations (of order 15%) of genus dependent exponents from their asymptotic values. From the relation (5.9) we can conclude that there also must be small but significant deviations from linearity of $x(g)$ in the region $5 < g < 15$. This suggests that the slope of $x(g)$ should decrease with greater g ,

so that the above estimate of the slope (1.25) may be too large. Still our data indicates that $x(g)$ is at least roughly linear in g ; presumably on larger lattices with better statistics, the systematic deviations we observe from linearity will decrease asymptotically with large g .

For the geometrical case, figure 5.16 shows that the relation between $\langle A \rangle$ and g is nearly linear already for small genus. The next plot (figure 5.17), showing $\ln(\langle A \rangle)$ vs. $\ln(g)$ indicates a small deviation for low genus. For $2 \leq g \leq 12$ we have $\langle A \rangle \simeq g^{0.95}$ which becomes $g^{0.99}$ for $12 \leq g \leq 24$. So we clearly see that asymptotically we will get a linear relation between $\langle A \rangle$ and g for the geometrical case.

We now return to a discussion of the data obtained for FK clusters on the SC lattice. Recall that generally our fits on the SC lattice have not been nearly as good as those for data taken on the BCC lattice. Indeed, the results for x and μ are also not nearly as clean as those obtained on the BCC lattice, but they do substantiate our preceding qualitative observations. In this respect, they are important in that they allow exhibit some degree of universality for our results. We first show the cosmological constant, computed from moments, as a function of genus in figure 5.18. Its variation with genus is very small, being compatible with a small downward drift superimposed on constant behavior of about 0.015. Thus, a handle occurs roughly every 60 plaquettes. Note that we expect a larger cosmological constant on this lattice than on the BCC lattice, since the SC lattice contains fewer plaquettes per unit volume.

$x(g)$ also exhibits larger transient effects (due to lattice artifacts and finite-size effects) on the SC lattice than on the BCC lattice. In the figure 5.19, we plot $x(g) - x(g - 1)$ for g up to 15. This difference systematically decreases up to genus 7 or 8 (corresponding to significant curvature in the behavior of $x(g)$ vs. g for small g) and then seems to level off somewhat. In fact, at this point, the slope appears to be about 1.25. For small genus, $g \simeq 15$, we find that roughly $\langle A \rangle \simeq g^{.82}$, with the exponent systematically and slowly increasing with g . Presumably, again, one would then expect that the slope of $x(g)$ also decreases with increasing g . Therefore, though the SC data is somewhat noisier and more susceptible to lattice artifacts, we find that even the deviations from asymptotic behavior that it exhibits are quite similar to those measured on the BCC lattice.

Our results for μ and $x(g)$ for percolation on the SC lattice are again quite similar. As the figure 5.20 demonstrates the cosmological constant does not show much variation with genus (it is again approximately 0.015, but it does exhibit a small transient downward shift). The plot of $x(g) - x(g - 1)$ in figure 5.21 resembles the one obtained in the Ising SC case, though it is even more noisy. We find for small genus roughly $\langle A \rangle \simeq g^{.81}$ with again an exponent that increases slowly with genus.

We also examined the behavior of the constant of proportionality C_g in our fits to see if it is asymptotically compatible with the result predicted by the Poisson scenario,

$$C_g = C \frac{\mu^g}{g!}. \quad (5.10)$$

In the figure 5.22, we plot $\ln(C_g) + \ln(g!) - g\ln(\mu)$ vs. g for fits to FK cluster data on the $L = 64$ BCC lattice. This figure indicates that C_g decays more quickly than in equation (5.10) up to about genus 10. Beyond that, the curve plateaus fairly abruptly, indicating that the form of C_g is indeed consistent with the Poisson prediction above genus 10. We find qualitatively identical results when we plot the same quantity extracted from FK cluster SC lattice data and pure percolation data. Again C_g decays more quickly than Poisson indicates for small g but is again compatible with the Poisson scenario above genus 10.

As usual, a deviation from eq. (5.10) is expected for low genus. Otherwise, for small g , $N(g)$, obtained by integrating the area dependence of $N_g(A)$ would behave like

$$N(g) \simeq C_g \frac{\Gamma(x(g) - 1)}{\mu^{x(g)}}. \quad (5.11)$$

Since the slope of $x(g)$ is greater than one in this regime, $N(g)$ would increase with the genus if (5.10) were correct. Such an increase is certainly not present, thus $\ln(C_g) + \ln(g!) - g\ln(\mu)$ decreases initially. For larger genus, the plateau is roughly consistent with an asymptotic slope of 1 for $x(g)$.

For geometrical clusters the situation is different, see figure 5.23 As above, $\ln(C_g) + \ln(g!) - g\ln(\mu)$ first decreases up to genus 4. Then this quantity begins to grow, which seems consistent with a slope of $x(g)$ that is less than 1 and our observed behavior of $N(g)$ (which we discuss next). Here we do not really see a plateau, though the statistical errors are very large for high genus data.

There is another ansatz which perhaps better fits the genus dependence of C_g . It was already mentioned that the deviation of C_g from (5.10) is due to the fact that $x(g)$ deviates from g . In the figure 5.24, we compare these deviation by displaying $\ln(C_g) + \ln(g!) - g\ln(\mu)$ and $(g - x(g))$ together. On this plot, we see that despite large statistical errors, there is an exact proportional relation between $(g - x(g))$ and $\ln(C_g) + \ln(g!) - g\ln(\mu)$. This indicates that (5.10) could be changed to

$$C_g = C(e^\beta)^{g-x(g)} \frac{\mu^g}{g!} \quad (5.12)$$

with β the constant of proportionality (which is close to 10 in our case.) Of course, the above relation reduces to the Poisson prediction when the slope of $x(g)$ is 1.

By inserting (5.12) in (5.6), we have :

$$N_g(A) = C \frac{(e^\beta \mu)^g}{g!} \left(\frac{A}{e^\beta}\right)^{x(g)} e^{-\mu(g)A} \quad (5.13)$$

If we now redefine $m = e^\beta \mu$ and $a = \frac{A}{e^\beta}$ then this modified ansatz can be expressed simply as

$$N_g(A) = C \frac{m^g}{g!} a^{x(g)} e^{-ma}. \quad (5.14)$$

This ansatz reduces to the Poisson prediction only when the slope of $x(g)$ is 1. If we assume the above form (5.12) for C_g together with a linear dependence of $x(g)$ with slope not equal to 1, then the sum of $N_g(A)$ over g (which converges rapidly) will not asymptotically behave as a power law in A . This contradicts our earlier expectations and observations, based on the scaling behavior of $N(V)$ and $V \sim A$.

The Poisson scenario provides us with one further related prediction. It implies that asymptotically the number of surfaces of genus g , $N(g)$, should be proportional to $g^{-\tau}$. For the modified ansatz (5.12), $N(g)$ will only exhibit asymptotic power law behavior if and only if the slope of $x(g)$ is 1. In the next four figures (figures 5.25-5.28), we show log-log plots of the genus dependence of $N(g)$ for FK clusters and geometrical clusters on the BCC lattice and FK clusters and pure bond percolation on the SC lattice. In all four cases, these plots appear to be quite linear. Our fits for FK clusters on both the BCC and SC lattices yield a scaling exponent of 2.00 ± 0.01 in the region $6 \leq g \leq 24$. For the geometrical clusters, the scaling exponent is 2.02 ± 0.01 in the same region.

In this case, the results for percolation are a bit different. We observe a systematic upward drift in the exponent for low genus. For instance, on a window of $6 \leq g \leq 12$, we obtain an exponent of 1.90 ± 0.01 (as compared to 2.00 ± 0.01 for BCC FK, 1.99 ± 0.01 for SC FK clusters and 1.99 ± 0.01 for BCC geometrical clusters). The exponent is closer to the Ising exponent on higher genus windows, albeit with a large statistical error. For example, we obtain for percolation 1.98 ± 0.03 in the window $12 \leq g \leq 18$ (compared to 1.98 ± 0.02 for BCC Ising, 1.98 ± 0.05 for SC Ising and 2.06 ± 0.01 for BCC geometrical clusters) and 1.97 ± 0.05 in the window $18 \leq g \leq 24$ (compared to 1.98 ± 0.07 for BCC Ising, 2.03 ± 0.09 for SC Ising and 2.02 ± 0.02 for BCC geometrical clusters).

We definitely do observe power law behavior (as predicted by Poisson) but our exponents consistently are roughly 10 percent lower than τ (except in the case of geometrical clusters where the difference is only 5 percent); only in the case of bond percolation do we see any asymptotic upward drift in this exponent. Yet, given our experience with measuring other exponents in these systems, it seems reasonable that this discrepancy from Poisson could be attributed to systematic effects.

In conclusion, our genus data indicate that all scaling clusters examined satisfy the ansatz (5.6) with a nearly constant μ and an exponent x that asymptotically appears to depend linearly on g . We do, though, observe variations in the slope of x from 1 and other deviations (in the behavior of the overall coefficient C_g , e.g.) from the Poisson scenario. It is unclear, though, whether these deviations are significant; they appear to be somewhat inconsistent with other observations. We also know that finite-volume effects can in some cases induce systematic deviations in our exponents of at least 15-20 percent. Still, for geometrical clusters, we do not directly observe large finite volume effects in the measurement of $x(g)$; its value is rather stable as L changes from 60 to 100. Perhaps larger scale simulations are needed to properly determine the asymptotic form of $x(g)$.

5.3 Loop Scaling and Blocked Spins

One might wonder if there is any characteristic of the geometrical clusters that reflects the Ising phase transition at T_c , rather than the percolation transition at T_p . This cannot be

a simple extensive property of the surfaces such as their total area or topology, as we have seen. Rather one needs a finer measure of their distribution, which in particular properly reflects surface roughness. We have found one such measure by taking cross-sections of the surfaces. Consider the ensemble of loops formed by the intersection of the set of cluster boundaries with an arbitrary two-dimensional plane. We have found that the distribution of lengths of these loops is sensitive to the critical dynamics of the Ising fixed point.

To begin, recall the three-dimensional structure of boundaries of geometrical clusters as T is increased beyond T_p , particularly to $T = T_c$. For $T > T_p$, two percolated clusters of opposite sign span the lattice. For T not so close to T_c , we expect that the characteristics of the Ising interaction will not influence the large-scale structure of these percolating clusters. The percolating clusters (assuming the transition at T_p is indeed in the universality class of pure percolation) should then be described by the ‘links, nodes and blobs’ picture developed for the infinite clusters of pure percolation in dimensions below $d_c = 6$ [9, 32]. In this description, the links form the thin backbones of the cluster; they are connected together at the nodes which occur roughly every percolation correlation length ξ . Most of the volume of the cluster lies in dangling ends emanating from the backbones. The backbones are not simply-connected. Rather, they contain fingers which fuse together to generate the handles that we measure, thus forming blobs with diameter up to size ξ .

A cross section of the boundaries of these networks of tangled thin tubes would presumably be composed of a set of small lattice-sized loops. To check this, we examined the phase boundaries between up and down spins on planar slices of both the SC and BCC lattices. In figure 5.29, we show a log-log plot of $N(l)$, the number of loops of length l , versus l taken at the percolation temperature $\beta_p = .232$ on the SC lattice. The curve exhibits a sharp drop-off, indicating indeed that these slices contain only small loops. As we dial the temperature up towards T_c , we find that larger loops begin to appear in the slices. In figure 5.30, we present a ‘movie’ of four consecutive slices at T_c . Loops that are small, large and intermediate sized are present in each of these slices. In fact, at T_c , we find loops at all scales; $N(l) \sim l^{-\tau'}$! This scaling is depicted in the log-log plot in figure 5.31. As in figure 5.1, we observe a small bump at the end of the distribution followed by a rapid drop-off. These deviations from

scaling are again due to the influence of the finite-size of the lattice on the largest loops. All of the largest loops must bound the two percolating clusters, since there are no intermediate size geometrical clusters at T_c . The loops themselves have a non-trivial fractal structure; we determined that the number of sites enclosed within a loop of length l scales as $A(l) \sim l^{\delta'}$.

From these measurements, we estimated that $\tau' = 2.06(3)$ and $\delta' = 1.20(1)$. These values are probably not very accurate, however. As in the determination of τ from the behavior of $N(V)$, corrections to scaling and finite-size effects are a source of large systematic errors. These systematic effects were only of order 1 – 2% for δ ; thus we suspect that our estimate of δ' is considerably better than that of τ' . Carrying out these measurements also required a resolution of certain ambiguities. In particular, since the boundaries of domains self-intersect on slices of the cubic lattice, we had to pick a prescription (effectively another short-distance regularization) to define loops. Additionally, the enclosed area is not well-defined for loops that wind around the (periodic) lattice. We thus chose to exclude loops with non-zero winding number from consideration. Also, we note that these measured values presumably suffer from large systematic corrections because they do not satisfy the relation $\tau' = 1 + \delta'$, which can be derived through scaling arguments⁸. This relation also holds for the corresponding indices that describe the distribution of self-avoiding loops that bound clusters in the 2- d Ising model at the Curie temperature. In that case, $\tau' \sim 2.45$. Finally, we found that the scaling behavior of loops on slices slowly disappeared as we continued to increase the Ising temperature. At $\beta = .18$ on $L = 150$ SC lattices, we observed that very large loops were again exponentially suppressed in the distribution $N(l)$.

Should we be surprised by the presence of this ‘loop scaling’ at T_c ? The following argument, due to Antonio Coniglio, indicates that this result is at least plausible [34]. First, note that in the $T \rightarrow \infty$ limit, the distribution of loops and geometrical clusters is that of pure site percolation with $p = .5$. For site percolation on the square lattice, $p_c \sim .59$ so that if only half the sites contain identical spins, then the distribution of loops and clusters should be governed by a finite correlation length. Now consider turning on the Ising couplings in

⁸ See section 4

the x and y directions. As the spins become correlated, the critical concentration⁹ needed for percolation should diminish. At the Curie temperature for the $2-d$ Ising model ($T_c^{d=2}$) this critical concentration decreases to .5 and geometrical clusters and their boundaries percolate. In two dimensions, this critical concentration cannot be less than .5, since generically two percolating clusters cannot span a single lattice [35]. Imagine next turning on the Ising coupling in the z direction while tuning the x and y couplings to remain at criticality. If the critical concentration remains .5 as the system reaches the $3-d$ Curie temperature, then one would find a scaling distribution of clusters and boundaries on $2-d$ slices. On the other hand, we cannot rule out the possibility that the critical concentration again increases above .5; then we would never expect to find scaling of loops on slices of the $3-d$ Ising model.

We also observed scaling behavior of loops on the BCC lattice. In particular, only small loops were found at T_p while scaling of $N(l)$ with the values $\tau' = 2.23(1)$ and $\delta' = 1.23(1)$ occurred at T_c . The uncertainty in the value of T_c probably leads to a significant systematic error in the estimate of these exponents. They do obey the anticipated relation $\tau' = 1 + \delta'$; δ' is not particularly far from the estimate extracted from the SC data. Note that on slices of the BCC lattice, which are triangular, there is no longer any ambiguity in the definition of loops. In this case, $N(l)$ apparently satisfies a power-law distribution, with a temperature-dependent exponent, for all $T > T_c$! This observation can be fully understood theoretically, since the percolation threshold on triangulated lattices equals .5. Therefore, we definitely expect to observe loop scaling at $T = \infty$ with scaling exponents characteristic of $2-d$ percolation ($\tau' \sim 2.05$ and $\delta' = 1$). Since lowering the temperature increases correlations between spins, we expect to find percolated clusters on slices for all T . For $T < T_c$, however, minority spins cannot percolate on $2-d$ slices because, as stated above, only one infinite cluster can span a lattice. Thus the minority spins and the loops that enclose them must percolate at T_c on $2-d$ slices of the $3-d$ Ising model on the BCC lattice. If we assume that this phenomenon is independent of the particular lattice type, then it follows that loop scaling should always occur at T_c . A similar situation occurs for the $2-d$ Ising model on the triangular lattice: one can argue that the distribution $N(l)$ again scales as a power law for

⁹Note that we can adjust the relative concentration of up and down spins by also adding a magnetic field.

all $T > T_c$ because $p_c = 1/2$ on triangulated lattices.

It also seems reasonable that the presence of loop scaling may be related to the vanishing of the surface tension of the Ising model at T_c . Antiperiodic boundary conditions in one direction (say \hat{z}) force the appearance of an interface transverse to \hat{z} . The surface tension vanishes when the free energy of a system with such anti-periodic boundary conditions equals the free energy of a system with periodic boundary conditions in z . Consider a slice through the lattice in the x - z plane; it cuts the interface along a loop that winds across the x -direction. Vanishing surface tension allows this loop to wander freely due to the unsuppressed surface fluctuations. Thus one expects to find that the probability distribution for this loop to have length l is not cut off at large l . Furthermore, the probability to find a loop of length l much larger than the linear size of the system L should not care whether the loop is topologically wound across x . Hence, vanishing surface tension and loop scaling should be related phenomena.

We now comment on the significance of this scaling. As we noted in the previous two sub-sections, the geometrical cluster boundaries do not in the least resemble surfaces (in the continuum limit) at T_p . The presence of large loops at T_c might indicate that the boundaries grow large long handles. A visual examination of successive slices qualitatively indicates that this is not so. Large loops seemingly always vanish after several consecutive slices. Indeed, it is difficult to envision a smooth surface that decomposes into a scaling distribution of loops along arbitrary slices.

It should also be noted that the exponent τ' is probably not directly related to the magnetic or thermal exponents of the $3-d$ Ising model. More generally, it may not be associated with the behavior of correlation functions of local operators in a unitary quantum field theory. This is true also for loops bounding clusters in the $2-d$ Ising model. For in all of these cases, the scaling of geometrical clusters is determined by the geometric effects associated with percolation as well as the long-range correlations due to Ising criticality. Still, this scaling law describes physics that in principle is observable, perhaps by counting domains in sections of crystals that lie in the universality class of $3-d$ Ising. It would thus be quite interesting to construct a theoretical scheme to compute (approximately) the value

of τ' . These loops are significantly ‘rougher’ than the corresponding boundaries in the 2- d Ising model, since the exponent δ' is lower here. They gain more kinetic energy because they are given an extra dimension in which to vibrate; perhaps this is responsible for their increased roughness.

Ideally, we would like to view these loops as string states that evolve in Euclidean time (perpendicular to the slices). Their dynamics is described by the transfer matrix determined from Boltzmann factors associated with their creation, destruction, merging and splitting. We have thus found that the ground state wave functional (string field) of this transfer matrix is peaked around configurations that describe a scaling distribution of loops. These loops seemingly bear little relation to free strings, though, because they interact strongly by splitting and joining every few lattice spacings¹⁰. This is why the entire history of the loop ensemble largely consists of a single surface, whose gross properties have little to do with the critical dynamics. One might hope that some sort of perturbative string description could still be viable if the strength of this interaction were just a short-distance artifact; i.e. if the string coupling diminished towards zero in the infrared. To gauge whether this is likely, we blocked spins in our simulations to measure the renormalization group flow of the operator that couples to the total Euler character summed over all cluster boundaries. In particular, during simulations on $L=128$ SC and BCC lattices, we blocked spins, using the majority rule and letting our random number generator decide ties. At each blocking level, we reconstructed clusters and boundaries and then measured the genus summed over surfaces. We present the results of this analysis in table 7; data was taken at $\beta_c = .221651$ on the SC lattice and $\beta_c = .0858$ on the BCC lattice.

The results are not so conclusive. In particular, since we lack a very precise determination of the Curie temperature on the BCC lattice, it is likely that by the final blocking the couplings have flowed significantly into either the high or low-temperature regimes. Thus, one should probably not take the increase in genus density in the final two blockings on the BCC lattice seriously. This effect is not a problem on the SC lattice, where we fortunately know the critical temperature (based on previous Monte Carlo Renormalization Group measure-

¹⁰In practice, this makes an analysis of the transfer matrix a formidable task.

ments) to very high accuracy. On the other hand, we suspect that the small L blocked values on the SC lattice may be unreliable, due to ambiguity in the definition of genus. We can at least infer that the genus density decreases a bit during the first few blockings, indicating that the coupling $\exp(-\kappa)$ does at least slowly diminish at the beginning of the RG flow. There is no clear indication, however, that the flow continues on to the weak string coupling regime. In fact, we would naively expect that this ‘genus’ operator is irrelevant, since it involves couplings between next–nearest neighbor spins. Hence, we would not anticipate that the genus would decrease dramatically upon blocking. One might also object to our choice of blocking scheme. Indeed, perhaps it might be more appropriate to somehow block the cluster boundaries themselves rather than the spins. In practice this would probably be technically difficult.

6 Assessment

The prospects for passing from the Curie point to the regime in which surfaces are weakly coupled are addressed in the work of Huse and Leibler [5]. They qualitatively map out the phase diagram of a model of self–avoiding surfaces with action (2.1). The large κ (large coupling to total Euler character) regime of their model lies in a droplet crystal phase, where the large percolated surface has shattered into a lattice of small disconnected spheres. Such a configuration maximizes the Euler density; it clearly does not correspond to a theory of surfaces. By estimating the free energy difference between phases, they argue that the transition to this droplet crystal is first order. Given this picture, there seems to be little evidence for the existence of a fixed point describing a weakly coupled theory of surfaces near the Curie point of the Ising model. Nevertheless, we cannot definitely exclude the possibility that there is still some path which we have not considered to a weak–coupling theory.

In conclusion, it appears that evidence of a continuum theory of surfaces has eluded us in our investigation of Ising cluster boundaries. We have found, however, that these cluster boundaries do exhibit an intriguing fractal structure that does not typically appear in models of lattice surfaces.

7 Acknowledgments

We would like to thank Stephen Shenker for essential discussions which led to our investigations. We also greatly benefitted from discussions and correspondence with Mark Bowick, Antonio Coniglio, Francois David, Bertrand Duplantier, John Marko, Pierre Pujol and Jim Sethna. We are also grateful to NPAC for their crucial support. This work was supported in part by the Dept. of Energy grants DEFG02-90ER-40560, DEFG02-85ER-40231, the Mathematical Disciplines Institute of the Univ. of Chicago, funds from Syracuse Univ., by the Centre National de la Recherche Scientifique, by INFN and the EC Science grant SC1*0394.

8 Appendix

We now discuss the derivation of the scaling relation 4.4, which asserts that $\tau = \delta + 1$. These arguments are meant to be descriptive, not mathematically rigorous. Consider a configuration of loops bounding clusters on a slice \mathcal{D} of size $R \times R$. For a visualization of these loops, see Fig. 5.30. As before, the mean area $A(l)$ within a loop of size l scales as l^δ ; the number of loops of size l , $N(l)$, is proportional to $R^2 l^{-\tau}$. These formulas are at least valid in the regime $1 \ll l \ll R^{2/\delta}$.

For λ slightly larger than 1, consider the quantity

$$F(\bar{l}, \lambda) \equiv \int_{\bar{l}}^{\lambda \bar{l}} N(l) A(l) dl \propto R^2 \bar{l}^\gamma \frac{\lambda^\gamma - 1}{\gamma}; \quad (8.1)$$

$\gamma \equiv \delta + 1 - \tau$. To a first approximation, F measures the area enclosed in loops of size between \bar{l} and $\lambda \bar{l}$. This correspondence would not be exact if, for instance, one of the loops of size \bar{l} were embedded in a loop of size $\lambda \bar{l}$. The loops are self-avoiding and tend to meander through the slice \mathcal{D} , so such an embedding is highly unlikely for λ close to 1. In this case, the over-counting due to these embeddings is negligible and F cannot be much greater than R^2 . It follows then that γ cannot be greater than zero, for otherwise the contribution from \bar{l}^γ would over-saturate this limit for large \bar{l} .

We now argue that likewise γ cannot be negative. Consider a fixed value of λ not necessarily very close to unity; e.g. $\lambda = 10$. If γ were negative, then for large \bar{l} , the area

enclosed within loops with $\bar{l} < l < \lambda\bar{l}$ would be a negligible fraction of the area of the entire slice. It follows from the self-similarity of the percolation clusters that this cannot be so. Let us take an arbitrary subdomain of extent $\bar{l}^{2/\delta} \times \bar{l}^{2/\delta}$. By self-similarity, there should generically exist a cluster that barely spans this subdomain; its surrounding loop should have size of order \bar{l} and will enclose a non-negligible portion of this subdomain¹¹. We can tile the slice \mathcal{D} with these subdomains; loops of size of order \bar{l} ($\bar{l} < l < \lambda\bar{l}$) will then cover a significant fraction of the entire slice. We thus conclude that $\gamma = 0$ and this scaling relation holds.

¹¹As is apparent from Fig. 5.30, the loops are fat. Clearly in their meanderings, they will cut off and surround large islands in the regions of the slice that they traverse.

References

- [1] A. Polyakov, Phys. Lett. B 82 (1979) 247; E. Fradkin, M. Srednicki and L. Susskind, Phys. Rev. D 21 (1980) 2885; C. Itzykson, Nucl. Phys. B 210 (1982) 477; A. Casher, D. Føerster and P. Windey, Nucl. Phys. B 251 (1985) 29; Vl. Dotsenko and A. Polyakov, *in* Advanced Studies in Pure Math. 15 (1987).
- [2] E. Brézin and V.A. Kazakov, Phys. Lett. B 236 (1990) 144; M.R. Douglas and S.H. Shenker, Nucl. Phys. B 335 (1990) 635; D. J. Gross and A. A. Migdal, Phys. Rev. Lett. 64 (1990) 127.
- [3] G. Parisi, in Proceedings of the Third Workshop on Current Problems in High Energy Particle Physics, John Hopkins Conference, Florence 1979; G. Parisi, J.-M. Drouffe and N. Sourlas, Nucl. Phys. B 161 (1979) 397; B. Durhuus, J. Frohlich and T. Jonsson, Nucl. Phys. B 240 (1984) 453; J. Ambjorn, B. Durhuus, J. Frohlich and P. Orland, Nucl. Phys. B 270 (1986) 457; M. E. Cates, Europhys. Lett. 8 (1988) 719.
- [4] F. David, Europhys. Lett. 9 (1989) 575.
- [5] D. Huse and S. Leibler, J. de Physique 49 (1988) 605.
- [6] M. Karowski and H. J. Thun, Phys. Rev. Lett. 54 (1985) 2556; R. Schrader, J. Stat. Phys. 40 (1985) 533.
- [7] M. Caselle, F. Gliozzi and S. Vinti, Turin Univ. preprint DFTT-12-93; Nucl. Phys. Proc. Suppl. B 34 (1994) 726.
- [8] F. David, Jerusalem Gravity (1990) 80.
- [9] D. Stauffer and A. Aharony, Introduction to Percolation Theory (Taylor and Francis, London 1992).
- [10] J. Cambier and M. Nauenberg, Phys. Rev. B 34 (1986) 8071.
- [11] C. M. Fortuin and P. W. Kasteleyn, Physica 57 (1972) 536.

- [12] A. Coniglio and W. Klein, *J. Phys. A* 13 (1980) 2775.
- [13] R.G. Edwards and A.D. Sokal, *Phys. Rev. D* 38 (1988) 2009; A.D. Sokal, in *Monte Carlo methods in statistical mechanics: Foundations and algorithms*, NY preprints based on lectures at the Troisième Cycle de la Physique en Suisse Romande, June 1989.
- [14] C. -K. Hu, *Phys. Rev. B* 29 (1984) 5103.
- [15] J.-S. Wang, *Physica A* 161 (1989) 149.
- [16] B. Duplantier, *J. Stat. Phys.* 49 (1987) 411; *Physica D* 38 (1989) 71; H. Saleur and B. Duplantier, *Phys. Rev. Lett.* 58 (1987) 2325.
- [17] J. Cardy, Lecture notes of Les Houches Summer School, 1994, cond-mat@babbage.sissa.it # 9409094
- [18] R. H. Swendsen and J.-S. Wang, *Phys. Rev. Lett.* 58 (1987) 86.
- [19] R. H. Swendsen and J.-S. Wang, *J. Phys. A* 13 (1980) 2775.
- [20] M. Hasenbusch and K. Pinn, Munster Univ. preprint MS-TIP-92-24.
- [21] S. Kirkpatrick, in *Ill-Condensed Matter*, ed. by R. Balian, R. Maynard and G. Toulouse (North-Holland, Amsterdam 1979) p.321.
- [22] B. Duplantier, private communication, unpublished
- [23] J. L. Cambier and M. Nauenberg, *Phys. Rev. B* 34 (1986) 8071
- [24] C. Vanderzande and A. L. Stella, *J. Phys. A* 22 (1989) L445
- [25] V. Dotsenko, G. Harris, E. Marinari, E. Martinec, M. Picco and P. Windey, *Phys. Rev. Lett.* 71 (1993) 811.
- [26] V. Dotsenko, G. Harris, E. Marinari, E. Martinec, M. Picco and P. Windey, *Proceedings of 1993 Cargèse Workshop*, to appear, [hep-th/9401129](https://arxiv.org/abs/hep-th/9401129).
- [27] G. Baker, B. Nickel, M. Green and D. Meiron, *Phys. Rev. Lett.* 36 (1976) 1351.

- [28] C. Domb, in *Phase Transitions and Critical Phenomena*, vol. 3, eds. C. Domb and M. S. Green (Academic Press, London 1974); J. Zinn-Justin, *J. Physique* 42 (1981) 783.
- [29] C. Itzykson and J. M. Drouffe, in *Statistical field theory and lattice gauge theory* (Cambridge Univ. Press, Cambridge, 1989).
- [30] J. Adler, Y. Meir, A. Aharony and A. B. Harris, *Phys. Rev. B* 41 (1990) 9183.
- [31] P. L. Leath, *Phys. Rev. B* 14 (1976) 5064.
- [32] P. G. DeGennes, *La Recherche* 7 (1976) 919.
- [33] G. Moore and P. Ginsparg, in *Recent directions in particle theory*, eds. J. Harvey and J. Polchinski (World Scientific, Singapore, 1993) pp. 537-588.
- [34] A. Coniglio, private communication.
- [35] A. Coniglio, C. R. Nappi, F. Peruggi and L. Russo, *J. Phys. A* 10 (1977) 205.

Figure Captions

Fig. 3.1 The Wigner–Seitz cell of the BCC lattice with next–nearest neighbor interactions.

Fig. 4.1 $\ln N(L)$ vs. $\ln L$ for geometrical clusters on the 1000×1000 triangular lattice.

Fig. 4.2 $\ln A(L)$ vs. $\ln L$ for geometrical clusters on the 1000×1000 triangular lattice.

Fig. 5.1 $\ln N(V)$ vs. $\ln V$ for FK clusters on the $L = 64$ SC lattice.

Fig. 5.2 The number of genus 1 surfaces at T_c as a function of dual surface area A for FK clusters on the $L = 64$ SC lattice, with a best fit to the functional form given in equation (5.6).

Fig. 5.3 As in the previous figure, but for genus 5.

Fig. 5.4 As in the previous figure, but for $3d$ bond percolation clusters.

Fig. 5.5 As in the previous figure, but for FK clusters on the $L = 64$ BCC lattice and for genus 2.

Fig. 5.6 As in the previous figure, but for genus 5.

Fig. 5.7 The number of genus 2 surfaces at T_p as a function of dual surface area A bounding minority (geometrical) clusters on the $L = 60$ BCC lattice.

Fig. 5.8 As in the previous figure, but for genus 5.

Fig. 5.9 The dependence of μ (extracted from the moments of the area distribution) on genus for FK clusters on the $L = 64$ BCC lattice at T_c .

Fig. 5.10 The dependence of μ (extracted from moments) on genus for surfaces bounding minority (geometrical) clusters on the $L = 60$ BCC lattice at T_p .

Fig. 5.11 The dependence of x (extracted from direct fits to (5.6) and moments) on genus for FK clusters on the $L = 64$ BCC lattice at T_c .

Fig. 5.12 The dependence of $x(g) - x(g-1)$ on genus for FK clusters on the $L = 64$ BCC lattice at T_c .

Fig. 5.13 The dependence of x (extracted from direct fits to (5.6) and moments) on genus for surfaces bounding minority (geometrical) clusters on the $L = 60$ BCC lattice at T_p .

Fig. 5.14 The dependence of $x(g) - x(g-1)$ on genus for surfaces bounding minority (geometrical) on the $L = 60$ BCC lattice at T_p .

Fig. 5.15 The dependence of $\ln(\langle A \rangle)$ on $\ln(g)$ for FK clusters on the $L = 64$ BCC lattice at T_c .

Fig. 5.16 The dependence of $\langle A \rangle$ on genus for surfaces bounding minority (geometrical) on the $L = 60$ BCC lattice at T_p .

Fig. 5.17 The dependence of $\ln(\langle A \rangle)$ on $\ln(g)$ for surfaces bounding minority (geometrical) on the $L = 60$ BCC lattice at T_p .

Fig. 5.18 The dependence of μ (extracted from the moments of the area distribution) on genus for FK clusters on the $L = 64$ SC lattice at T_c .

Fig. 5.19 The dependence of $x(g) - x(g-1)$ on genus for FK clusters on the $L = 64$ SC lattice at T_c .

Fig. 5.20 The dependence of μ (extracted from the moments of the area distribution) on genus for $3d$ bond percolation clusters on the $L = 64$ SC lattice.

Fig. 5.21 The dependence of $x(g) - x(g-1)$ on genus for $3d$ bond percolation clusters on the $L = 64$ SC lattice.

Fig. 5.22 The dependence of $\ln(C_g) + \ln(g!) - g \ln(\mu)$ on genus for FK clusters on the $L = 64$ BCC lattice at T_c .

Fig. 5.23 As in the previous figure, but for surfaces bounding minority (geometrical) clusters on the $L = 60$ BCC lattice at T_p .

Fig. 5.24 The dependence of $\ln(C_g) + \ln(g!) - g \ln(\mu)$ (\square) and $10 * (g - x(g))$ (\bullet) on genus for surfaces bounding minority (geometrical) clusters on the $L = 60$ BCC lattice at T_p .

Fig. 5.25 The dependence of $\ln(N(g))$ on $\ln(g)$ for FK clusters on the $L = 64$ BCC lattice at T_c .

Fig. 5.26 As in the previous figure, but for surfaces bounding minority (geometrical) clusters on the $L = 60$ BCC lattice at T_p .

Fig. 5.27 As in the previous figure, but for FK clusters on the $L = 64$ SC lattice at T_c .

Fig. 5.28 As in the previous figure, but for $3d$ bond percolation clusters on the $L = 64$ SC lattice.

Fig. 5.29 A log–log plot of the distribution of loops of length l on slices of an $L = 60$ SC lattice at T_p .

Fig. 5.30 Four consecutive slices of a representative configuration of geometrical clusters at T_c .

Fig. 5.31 A log–log plot of the distribution of loops of length l on slices of an $L = 150$ SC lattice at T_c .

Tables

(FKC = FK clusters, GC = Geometrical clusters, BP = $3d$ Bond percolation.)

| cluster type | lattice | size | no. of sweeps | β |
|--------------|------------|------|---------------|---------|
| GC | square | 500 | 100000 | 0.44068 |
| GC | square | 1000 | 25000 | 0.44068 |
| GC | triangular | 500 | 100000 | 0.27465 |
| GC | triangular | 1000 | 25000 | 0.27465 |
| GC | triangular | 500 | 100000 | 0 |
| GC | triangular | 1000 | 25000 | 0 |

Table 1: A record of the number of sweeps performed on two-dimensional lattices.

| cluster type | lattice | size | no. of sweeps | β |
|--------------|---------|------|---------------|----------|
| FKC | SC | 32 | 6000000 | 0.221651 |
| FKC | SC | 64 | 250000 | 0.221651 |
| FKC | BCC | 64 | 300000 | 0.0858 |
| GC | BCC | 30 | 500000 | 0.0959 |
| GC | BCC | 60 | 500000 | 0.0959 |
| GC | BCC | 100 | 50000 | 0.0959 |
| BP | SC | 32 | 50000 | – |
| BP | SC | 64 | 11000 | – |

Table 2: A record of the number of sweeps performed on three-dimensional lattices.

| cluster type | lattice | size | no. of sweeps | β |
|--------------|---------|------|---------------|---------|
| GC | SC | 60 | 40000 | 0.2216 |
| GC | SC | 150 | 4000 | 0.2216 |
| GC | BCC | 150 | 1000 | 0.0858 |

Table 3: A record of the number of three-dimensional configurations produced for an analysis of cross-sectional slices.

| interval of l | τ_{500} | δ_{500} | τ_{1000} | δ_{1000} |
|-----------------|--------------|----------------|---------------|-----------------|
| 40 — 2500 | 2.389 | 1.444 | 2.421 | 1.450 |
| 100 — 2500 | 2.382 | 1.445 | 2.419 | 1.451 |
| 40 — 1500 | 2.403 | 1.444 | 2.421 | 1.448 |
| 100 — 1500 | 2.396 | 1.445 | 2.416 | 1.450 |

Table 4: Square lattice, 500×500 and 1000×1000 .

| interval of l | τ_{500} | δ_{500} | τ_{1000} | δ_{1000} |
|-----------------|--------------|----------------|---------------|-----------------|
| 20 — 2500 | 2.431 | 1.454 | 2.440 | 1.452 |
| 100 — 2500 | 2.427 | 1.455 | 2.436 | 1.452 |
| 20 — 1500 | 2.438 | 1.454 | 2.444 | 1.454 |
| 100 — 1500 | 2.433 | 1.455 | 2.439 | 1.455 |

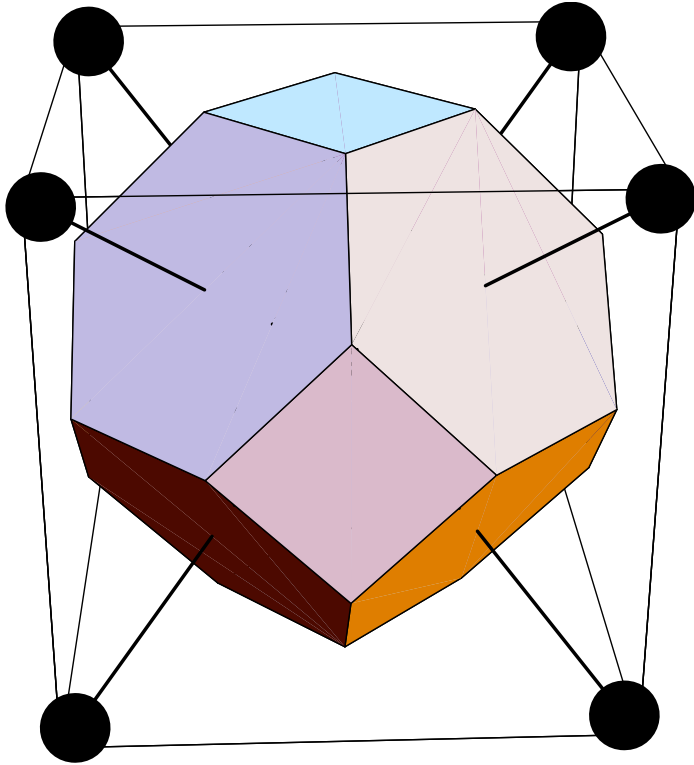
Table 5: Triangular lattice 500×500 and 1000×1000 .

| interval of l | $r_{l,500}^c$ | $r_{l,1000}^c$ | interval of l | $r_{l,500}^\infty$ | $r_{l,1000}^\infty$ |
|-----------------|---------------|----------------|-----------------|--------------------|---------------------|
| 100 — 800 | 2.471 | 2.471 | 200 — 800 | 2.219 | 2.218 |
| 200 — 800 | 2.472 | 2.471 | 300 — 800 | 2.218 | 2.217 |
| 100 — 1200 | 2.472 | 2.471 | 200 — 1200 | 2.220 | 2.218 |
| 200 — 1200 | 2.473 | 2.471 | 300 — 1200 | 2.220 | 2.218 |

Table 6: r_l for the 500×500 and 1000×1000 triangular lattices.

| lattice | 128 | 64 | 32 | 16 | 8 |
|---------|----------|----------|----------|----------|----------|
| BCC | .049 (3) | .039 (3) | .037 (3) | .039 (3) | .044 (3) |
| SC | .021 (2) | .020 (2) | .018 (2) | .015 (2) | .012 (1) |

Table 7: The mean genus per lattice site at T_c for blockings ($L = 8, 16, 32$ and 64) of an $L = 128$ lattice.



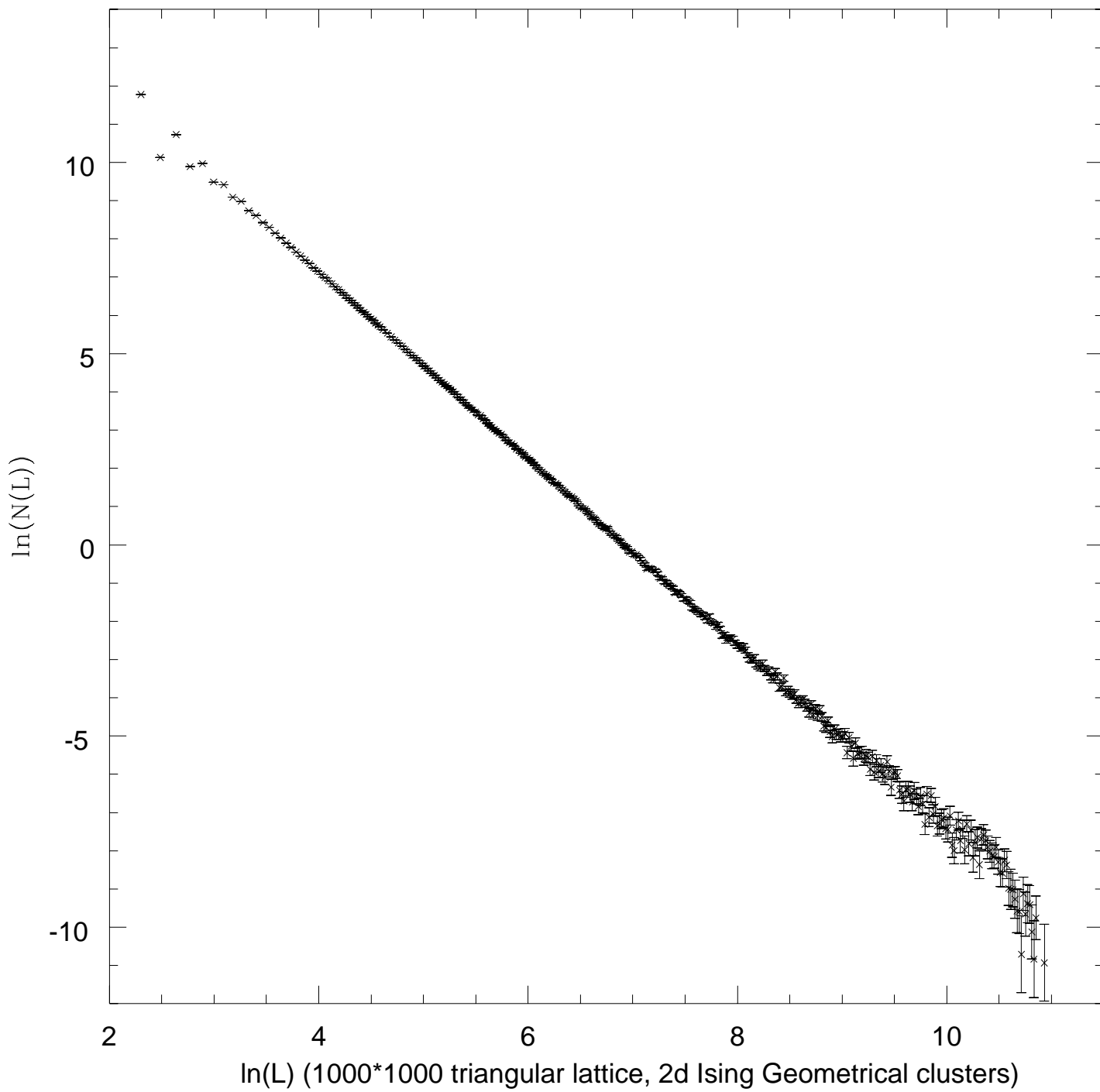


Figure 4.1

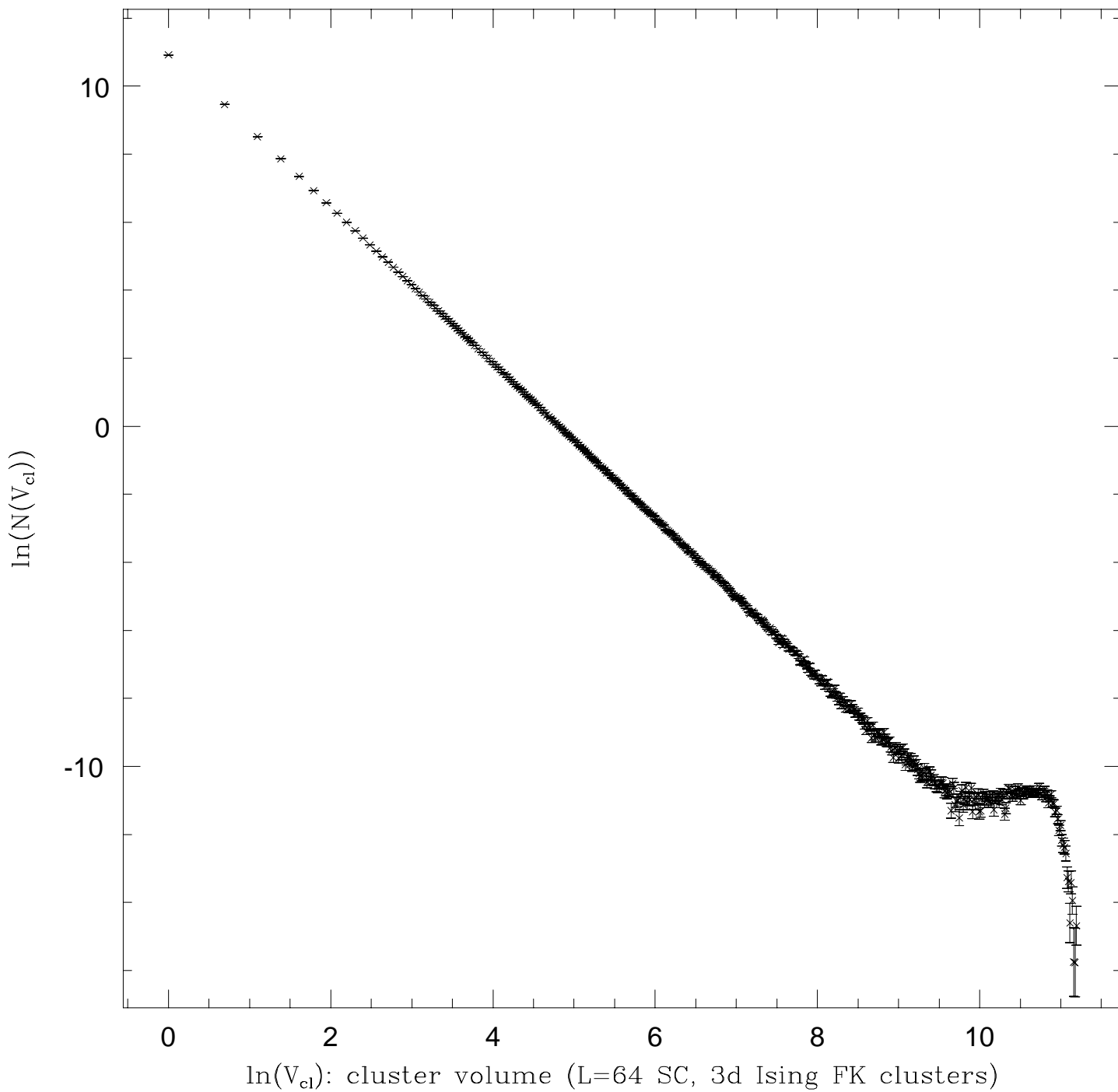


Figure 5.1

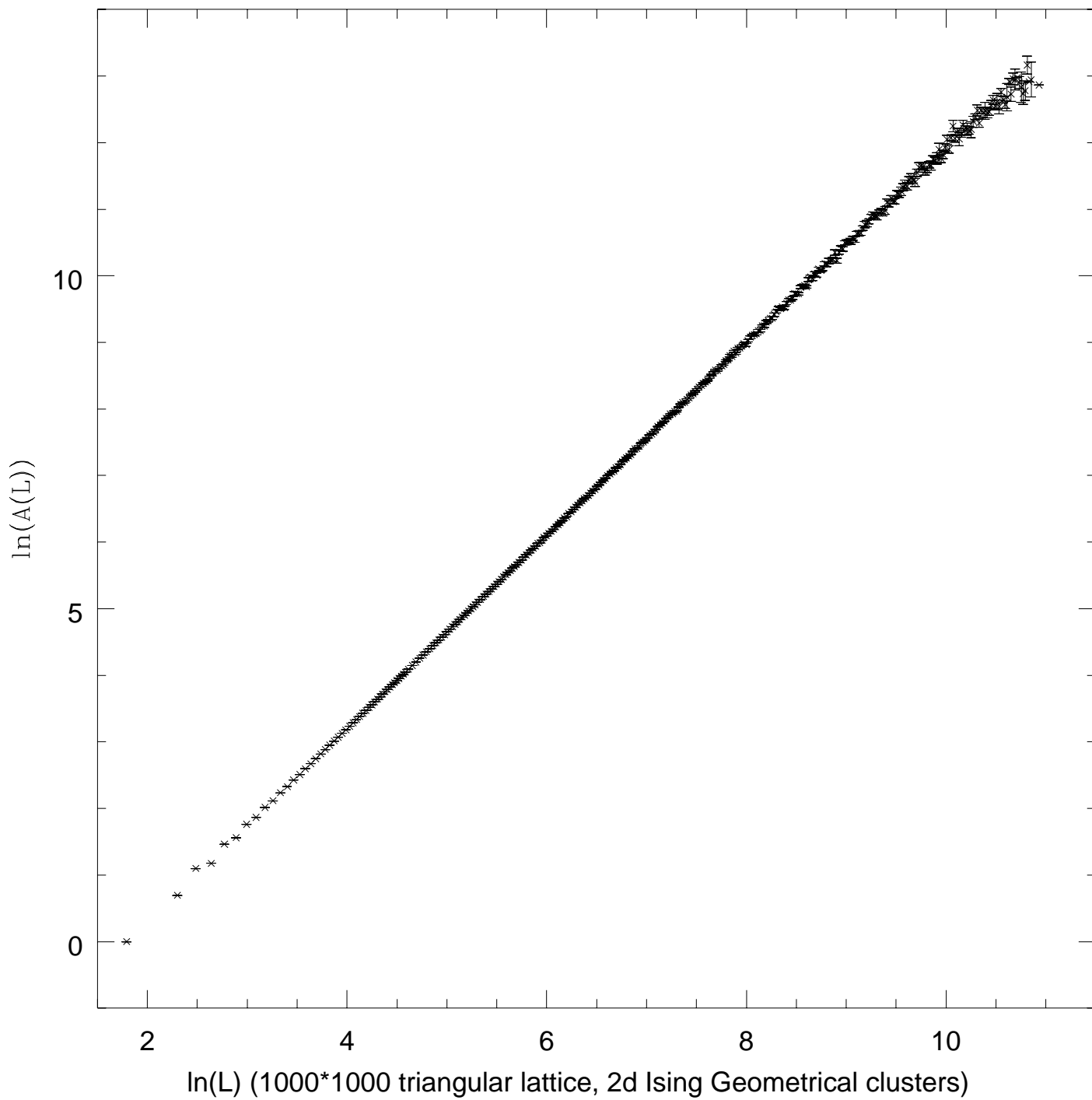
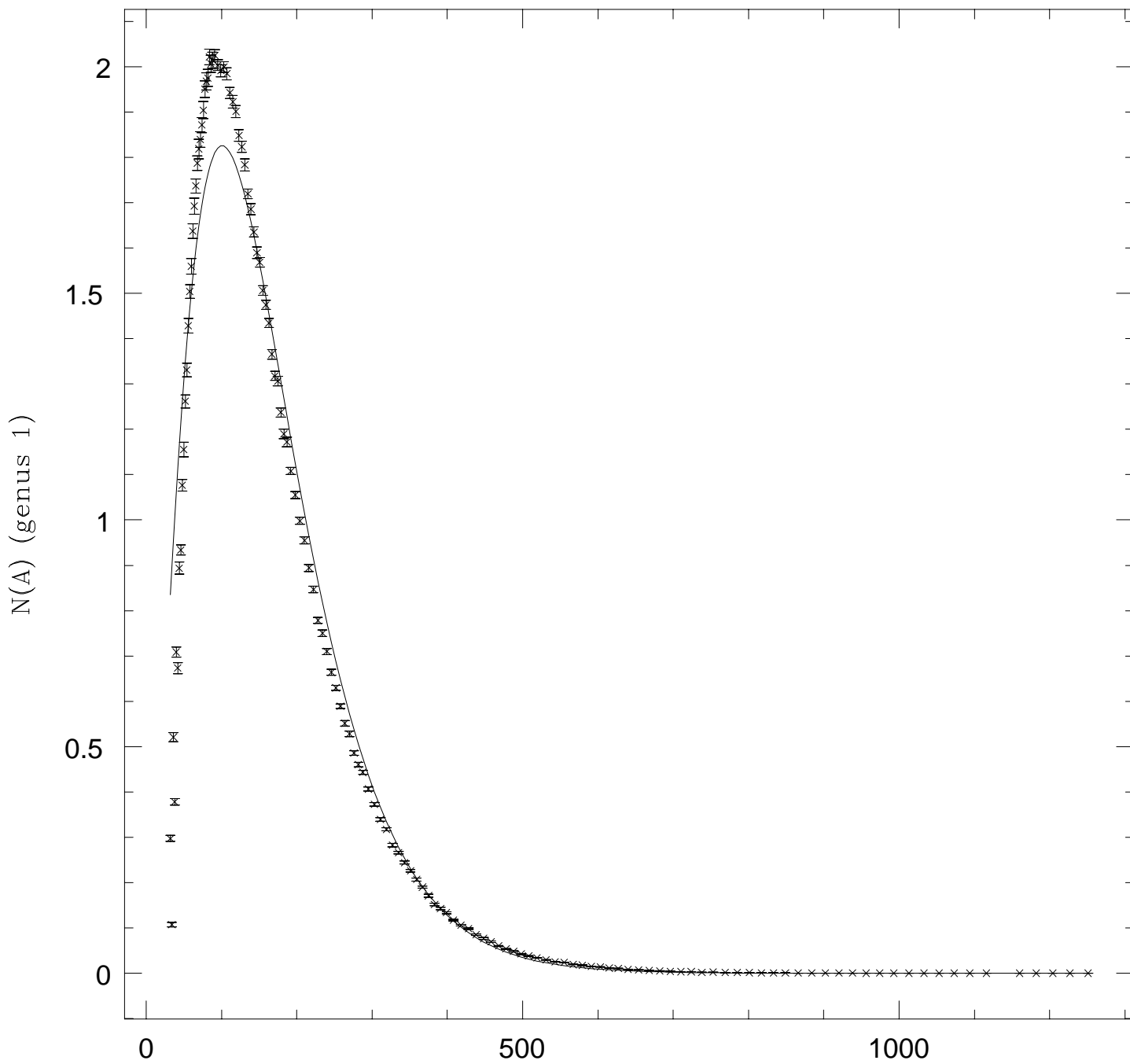
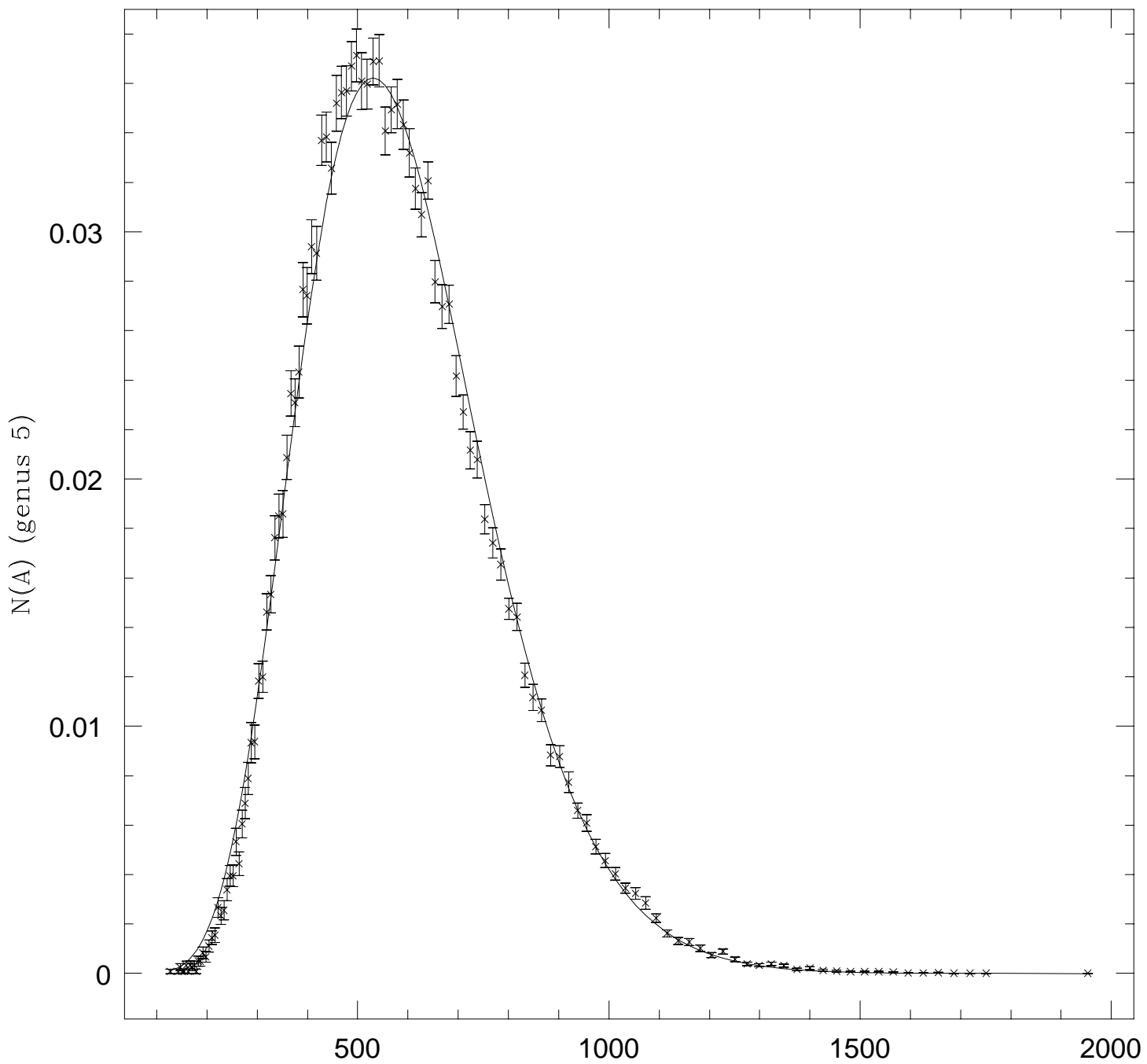


Figure 4.2



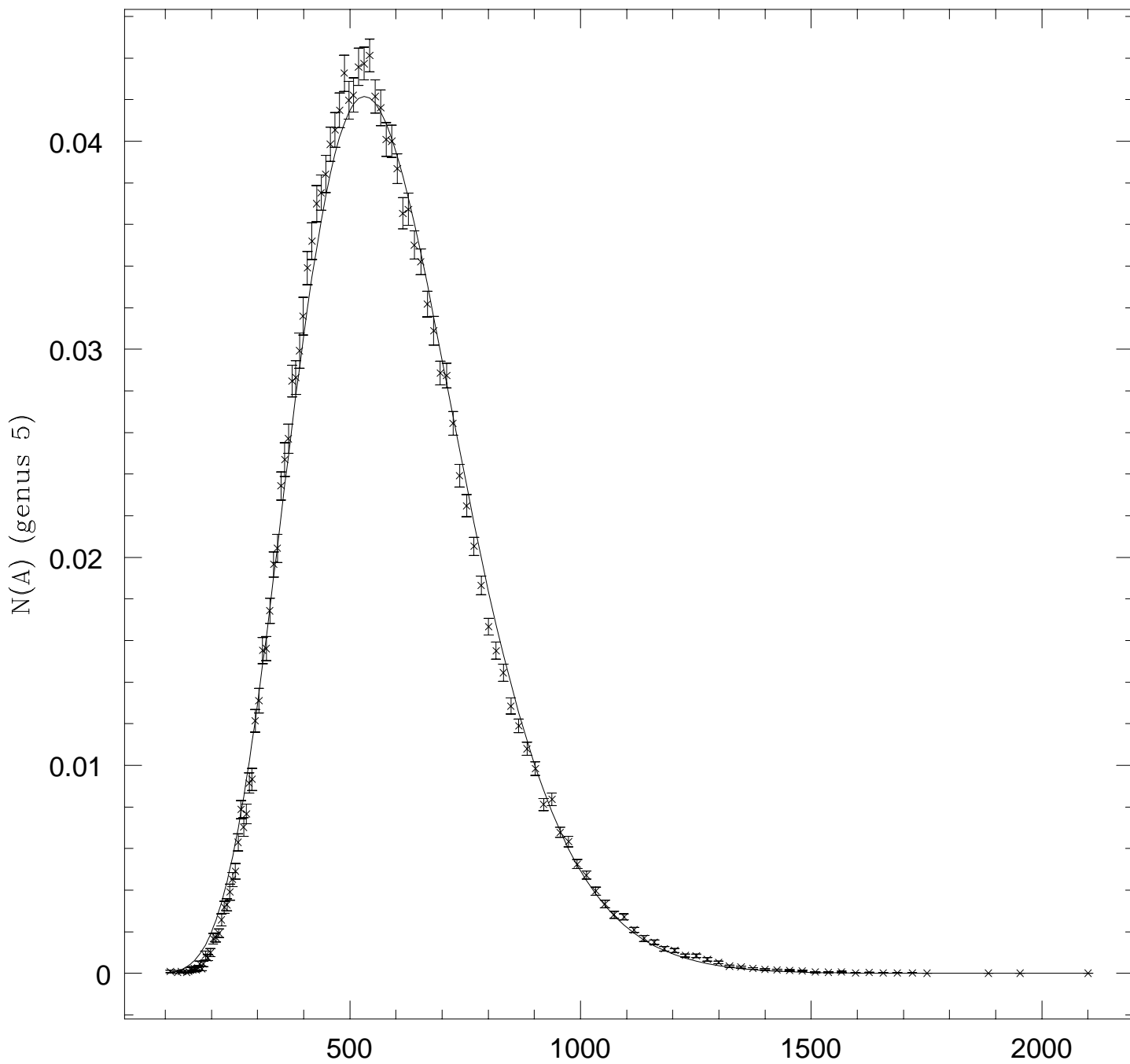
A: Dual Surface Area (L=64 SC, 3d Ising FK clusters)

Figure 5.2



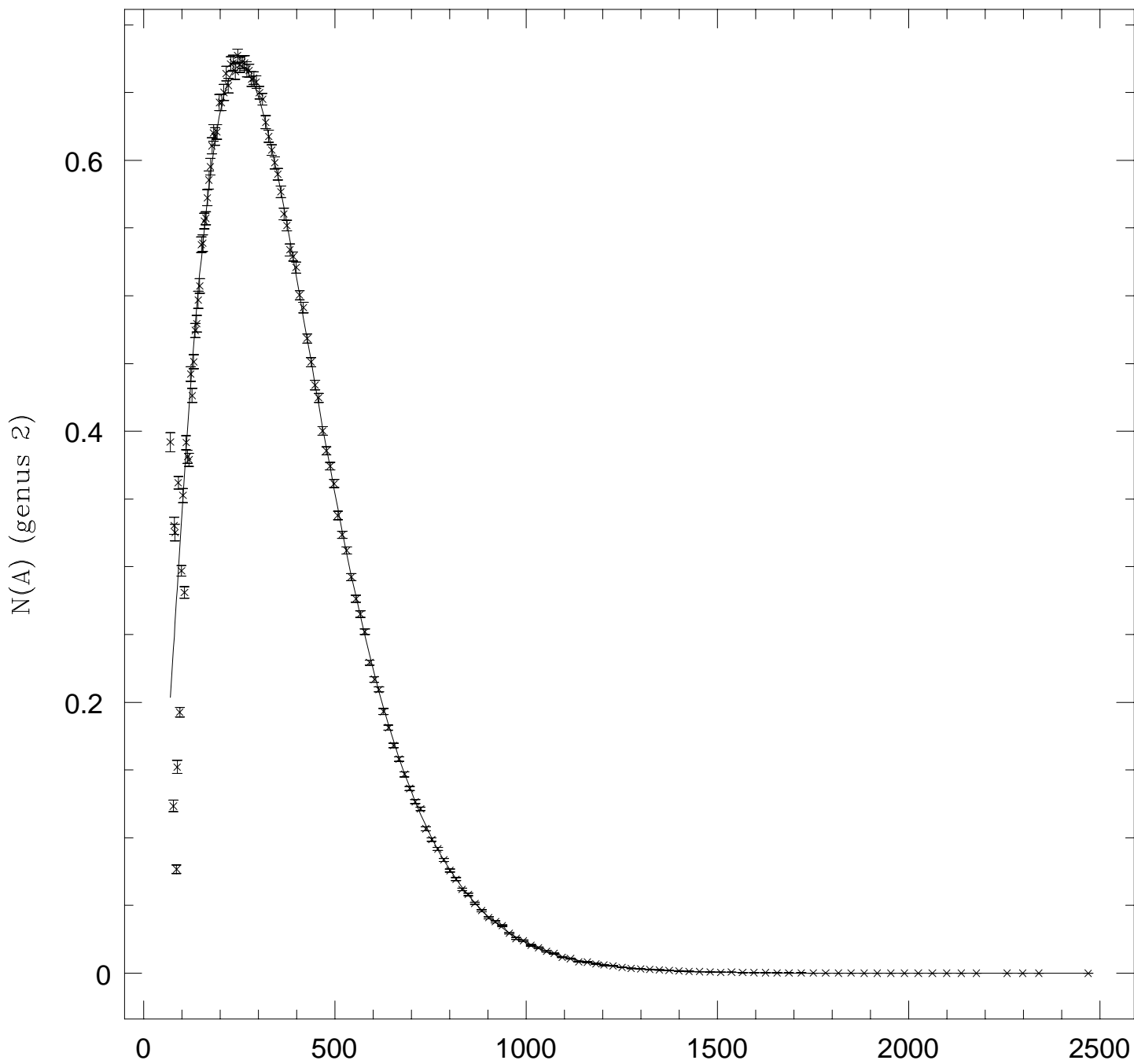
A: Dual Surface Area (L=64 SC, 3d Ising FK clusters)

Figure 5.3



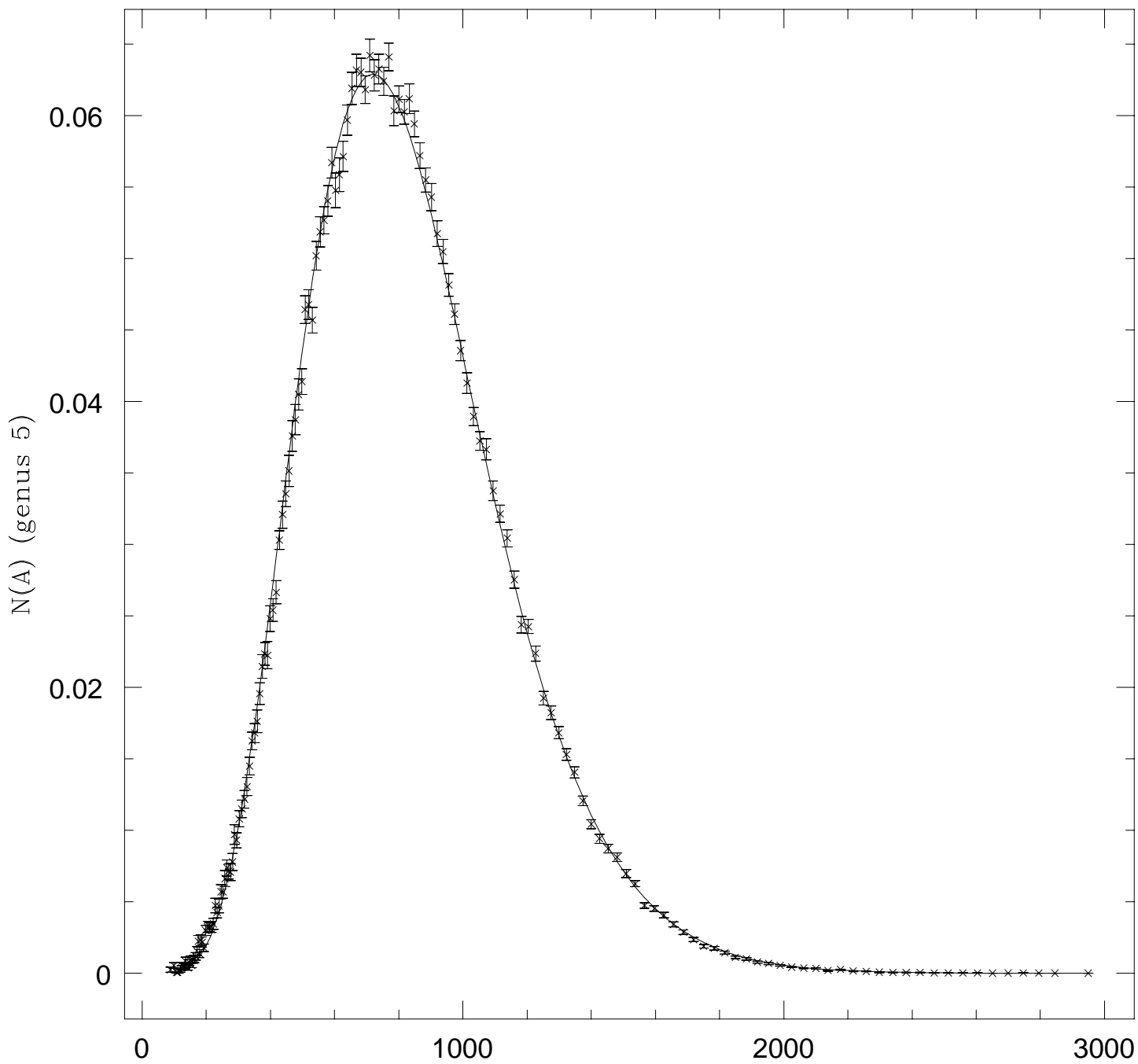
A: Dual Surface Area (L=64 SC, 3d Bond Percolation clusters)

Figure 5.4



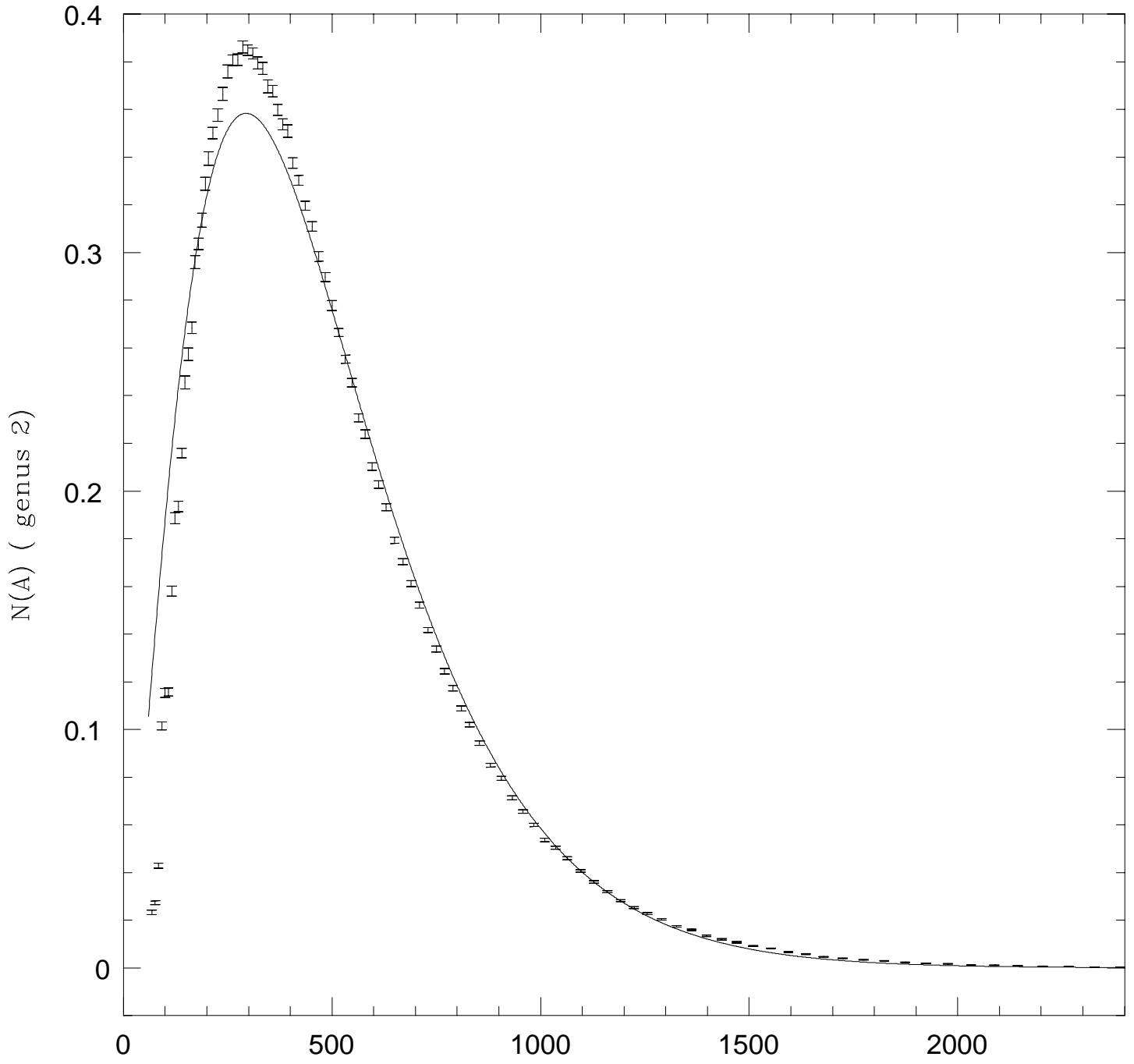
A: Dual Surface Area (L=64 BCC, 3d Ising FK clusters)

Figure 5.5



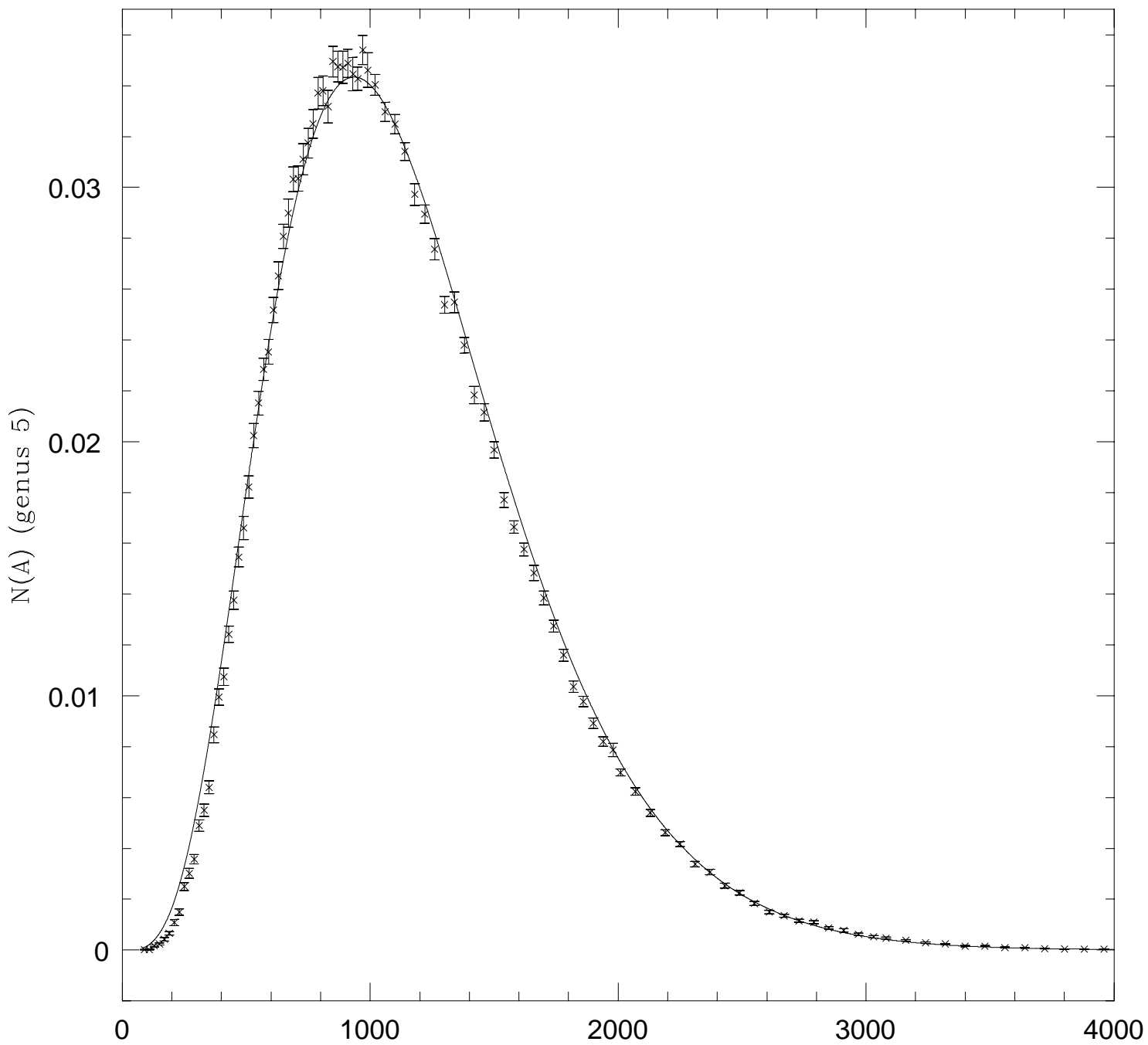
A: Dual Surface Area (L=64 BCC, 3d Ising FK clusters)

Figure 5.6



A: Dual Surface Area (L=60 BCC, 3d Ising geometrical clusters)

Figure 5.7



A: Dual Surface Area (L=60 BCC, 3d Ising geometrical clusters)

Figure 5.8

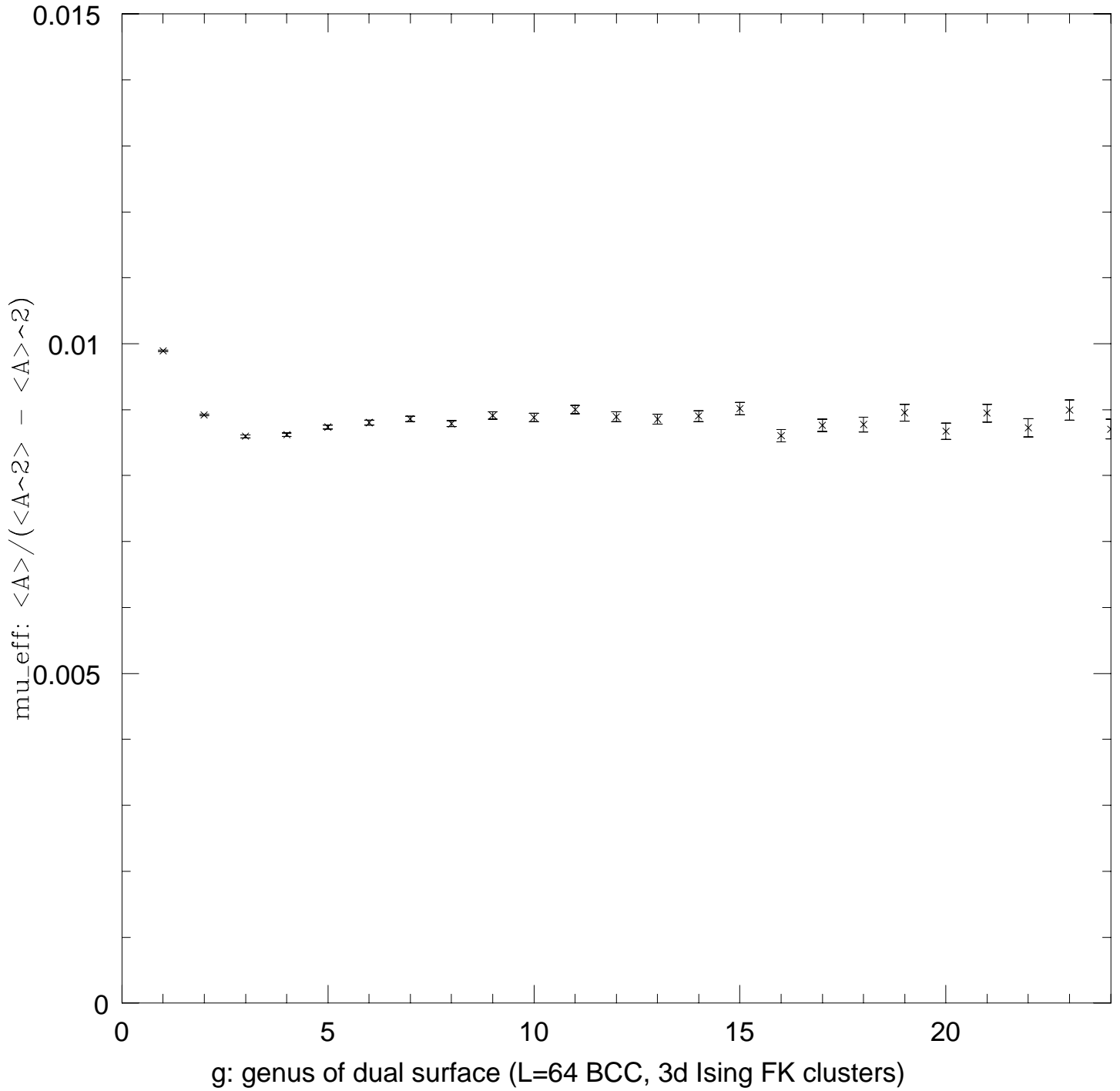


Figure 5.9

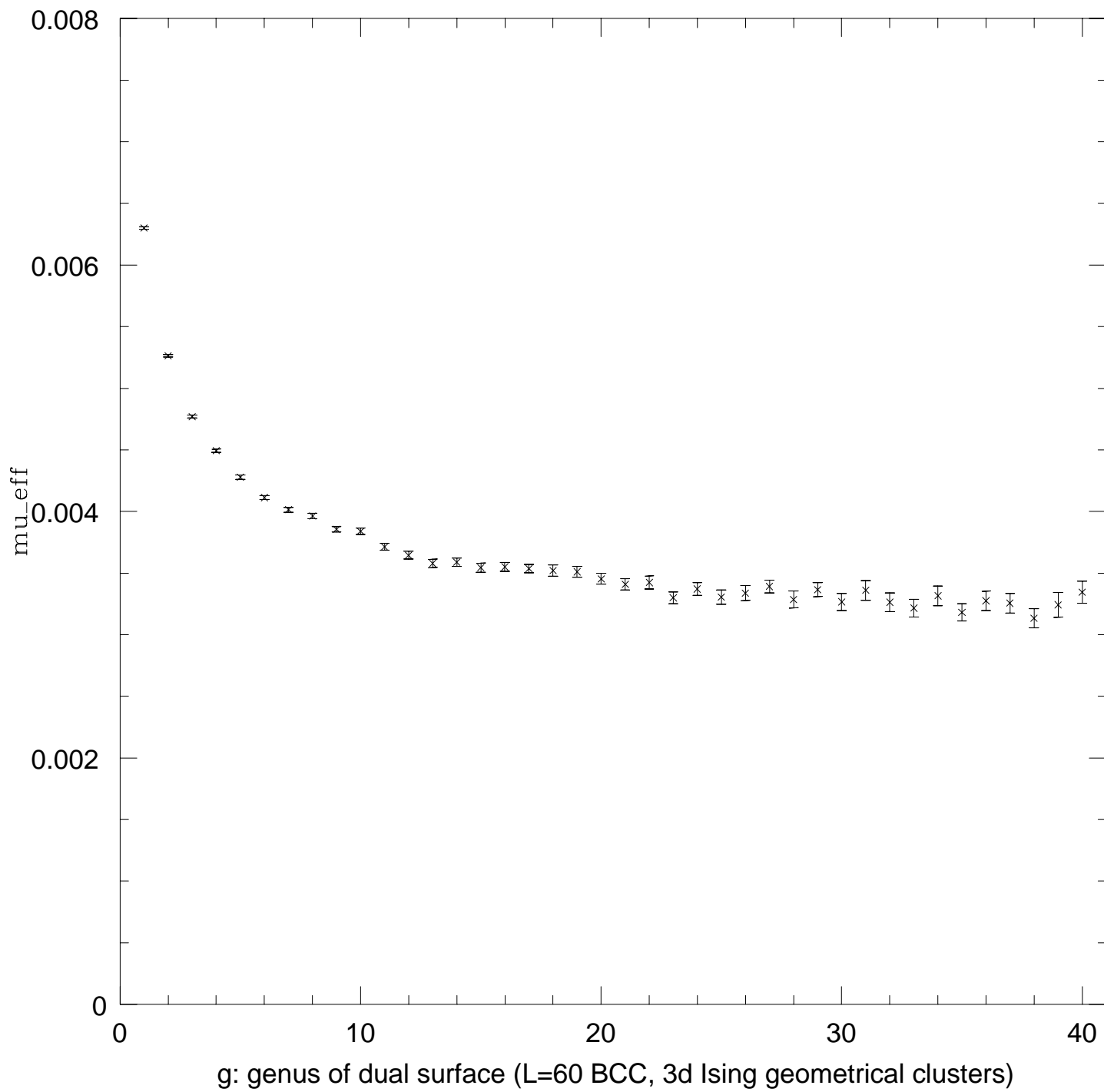


Figure 5.10

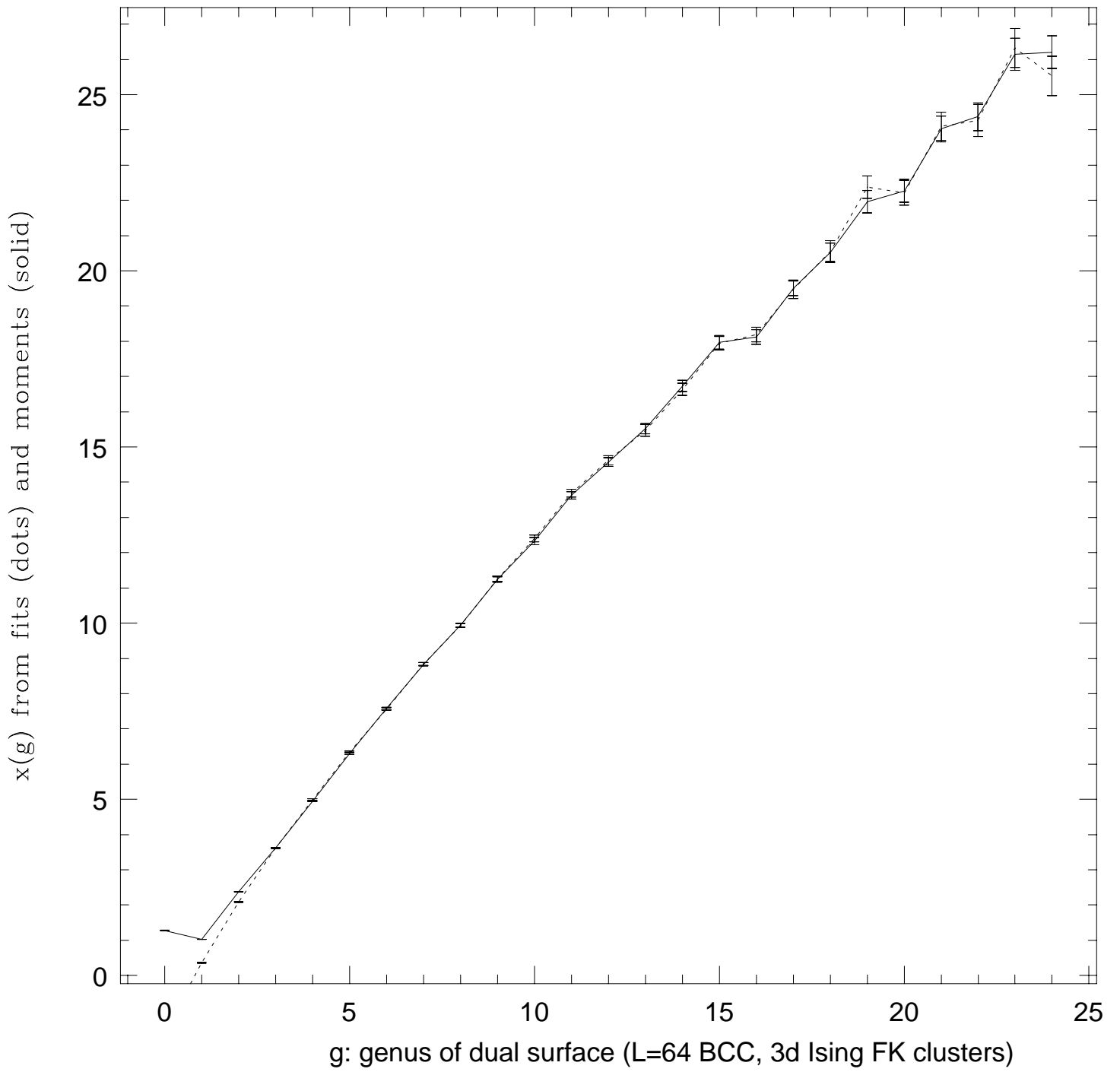


Figure 5.11

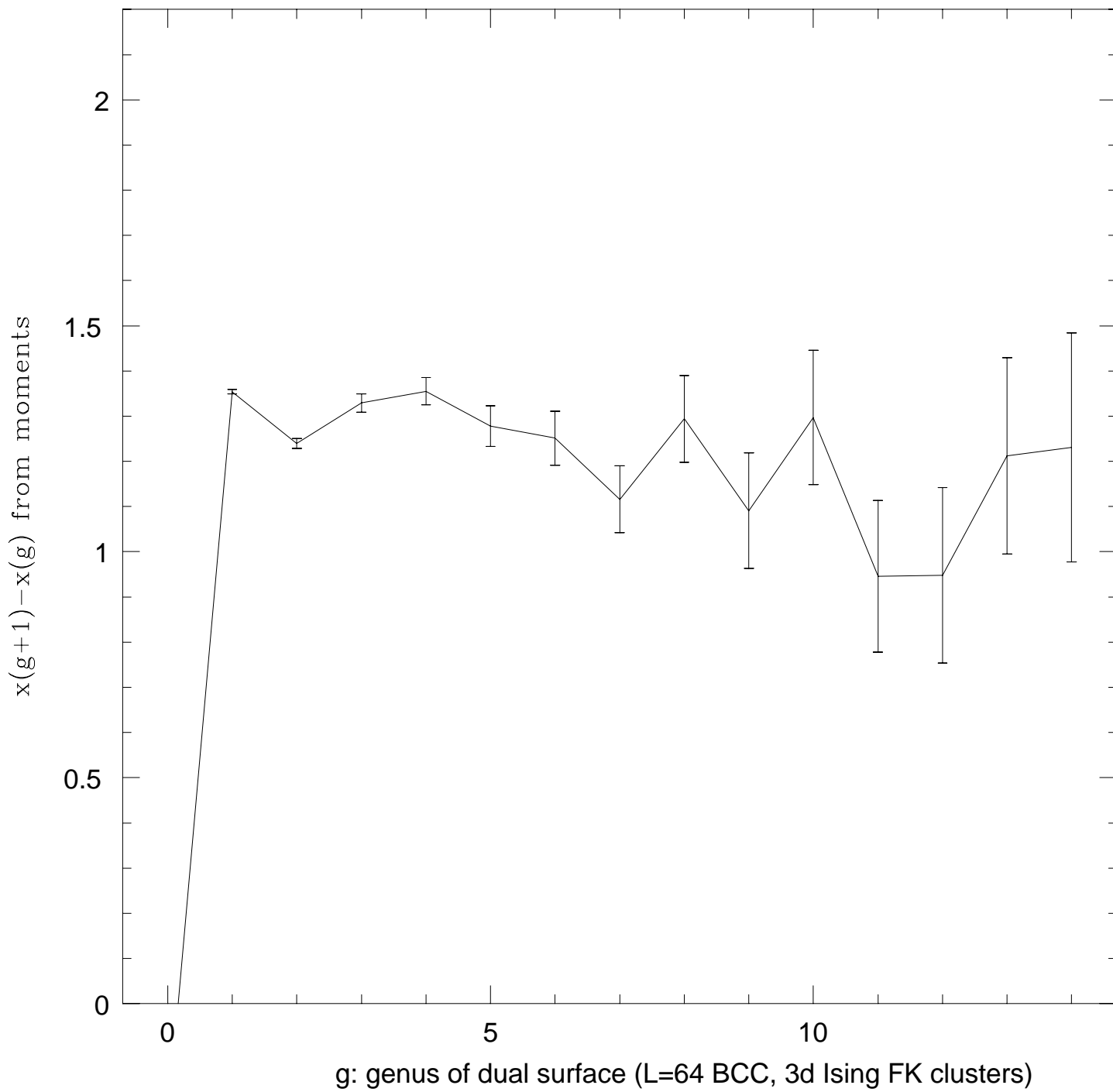


Figure 5.12

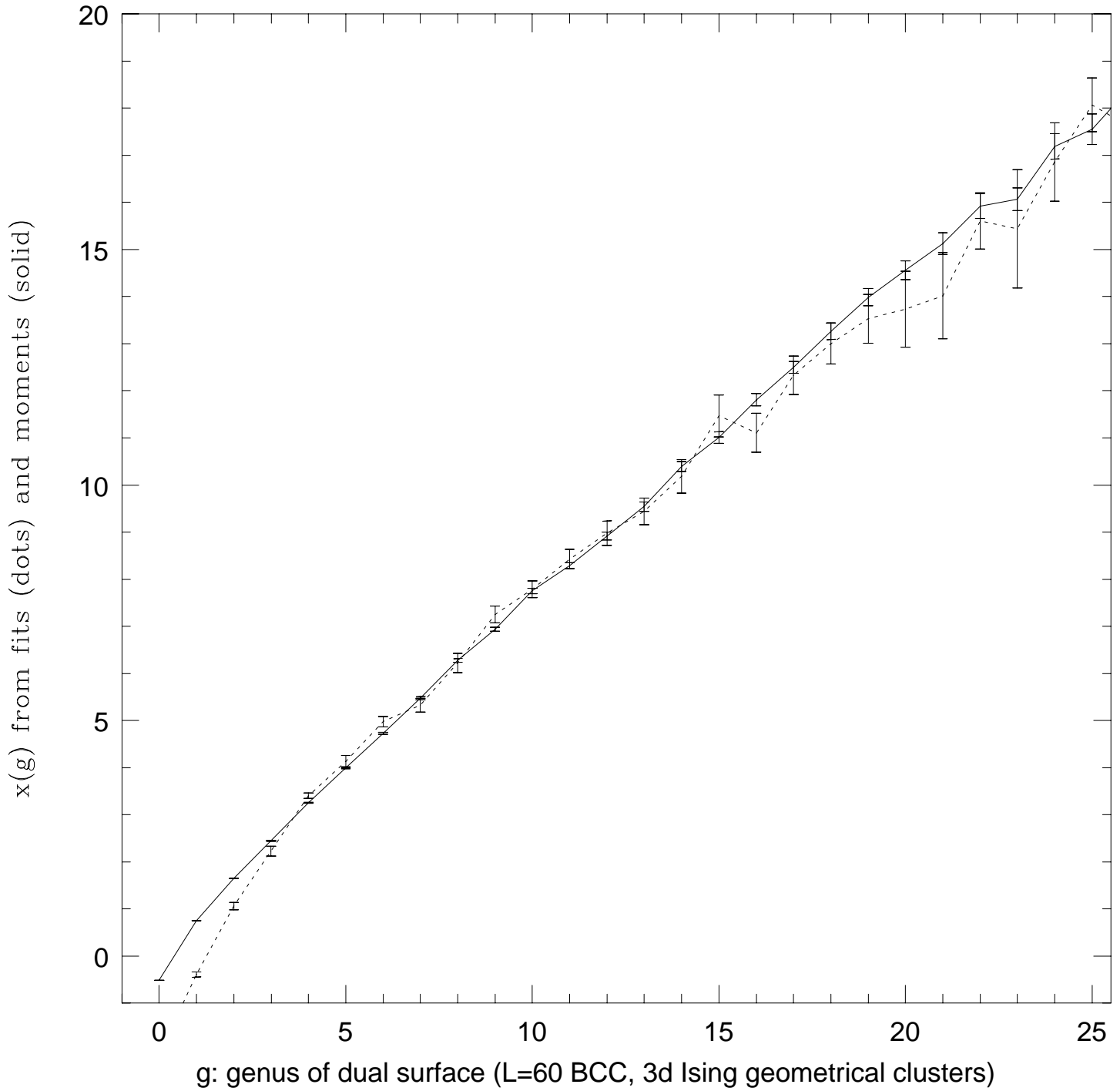


Figure 5.13

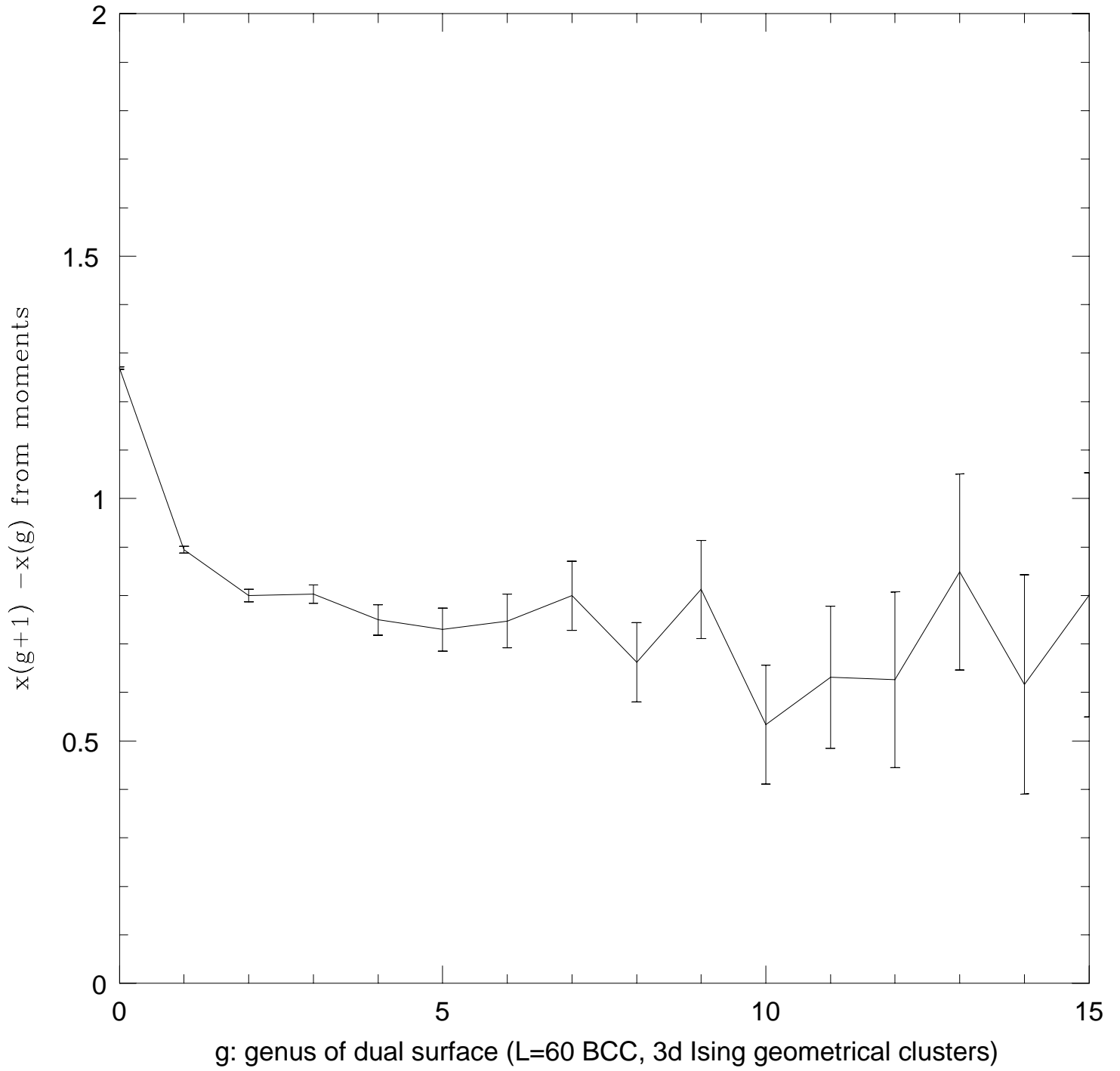


Figure 5.14

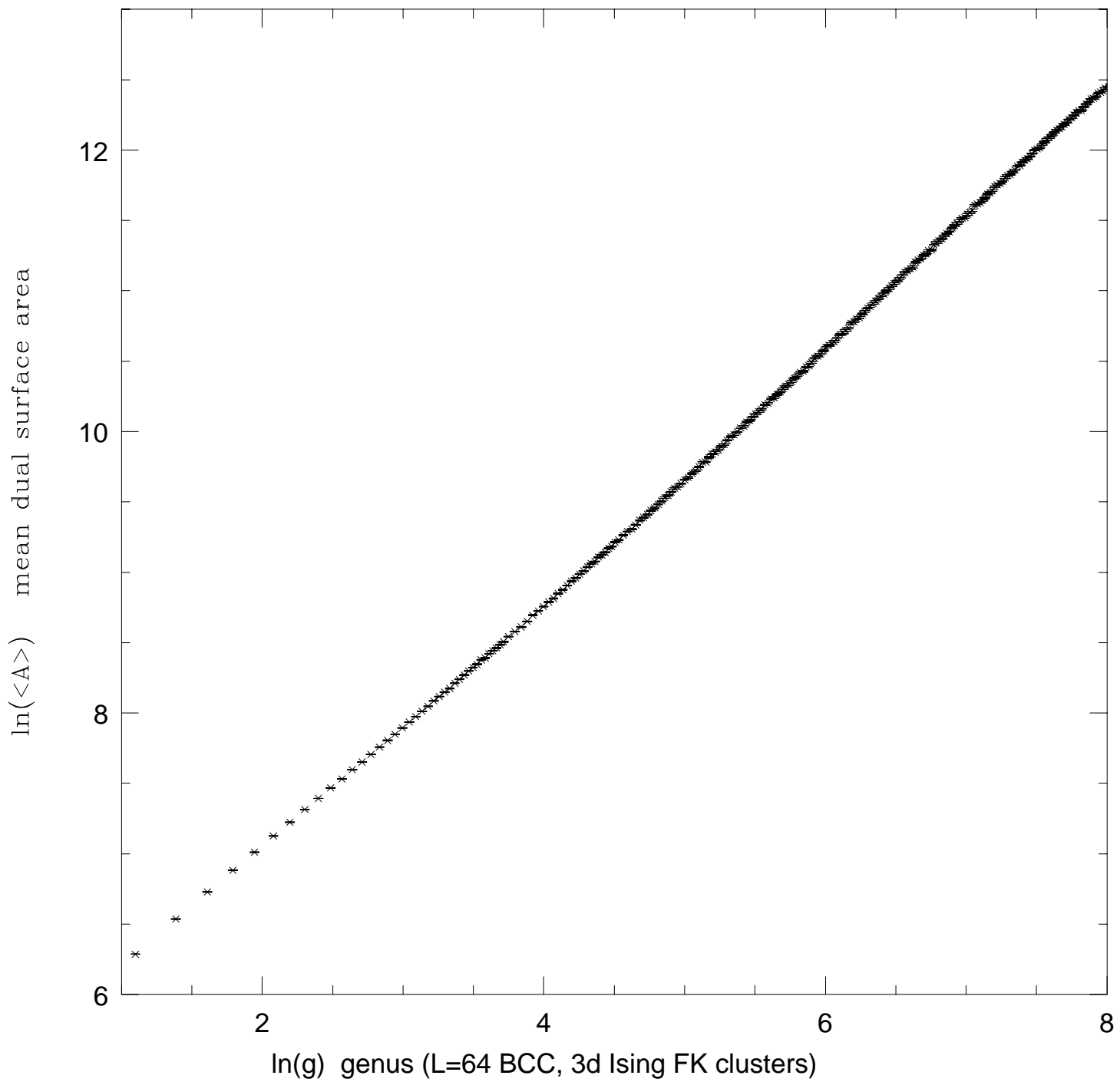


Figure 5.15

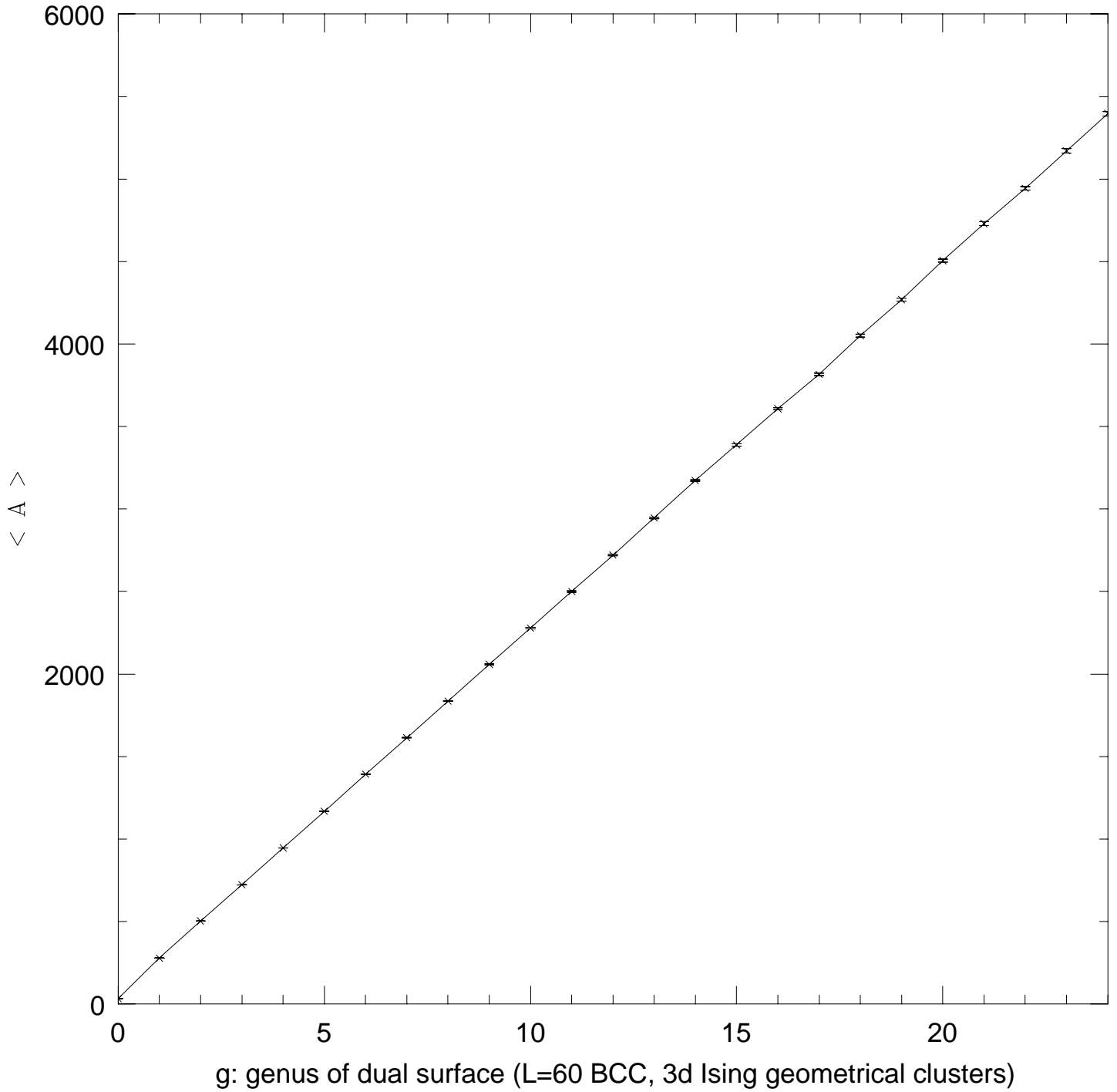
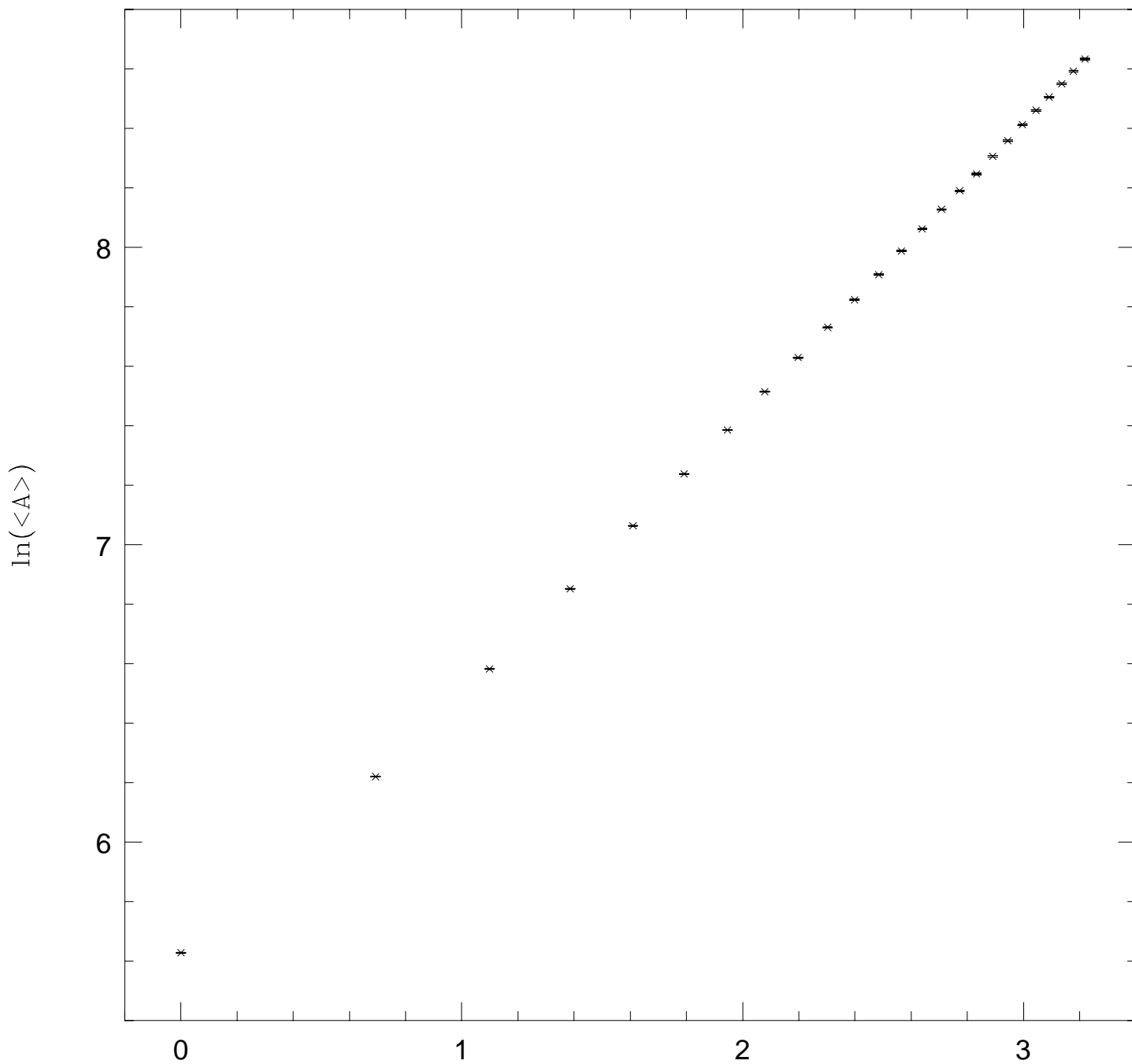


Figure 5.16



$\ln(g)$: log of the genus of dual surface (L=60 BCC, 3d Ising geometrical clusters)

Figure 5.17

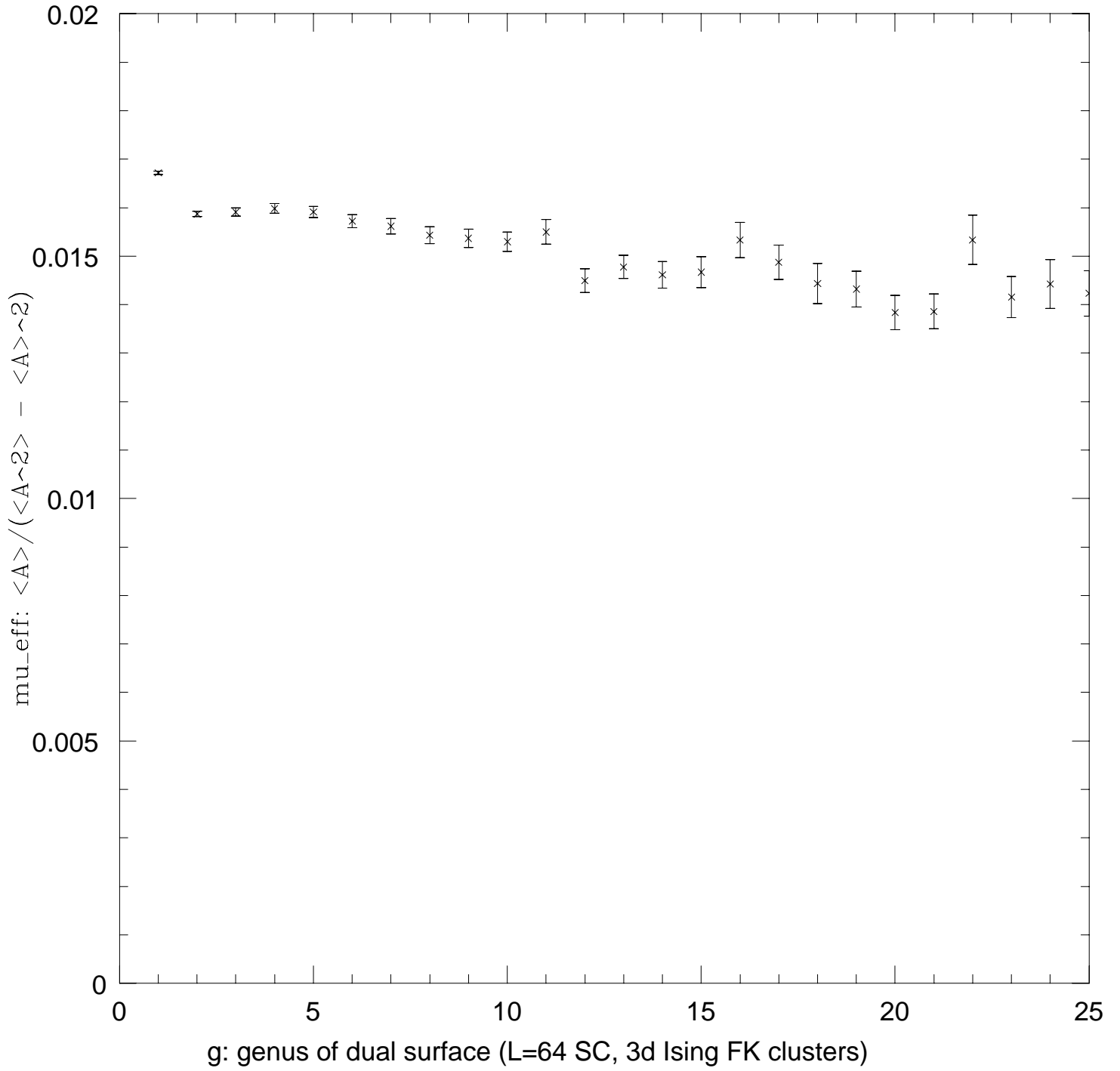


Figure 5.18

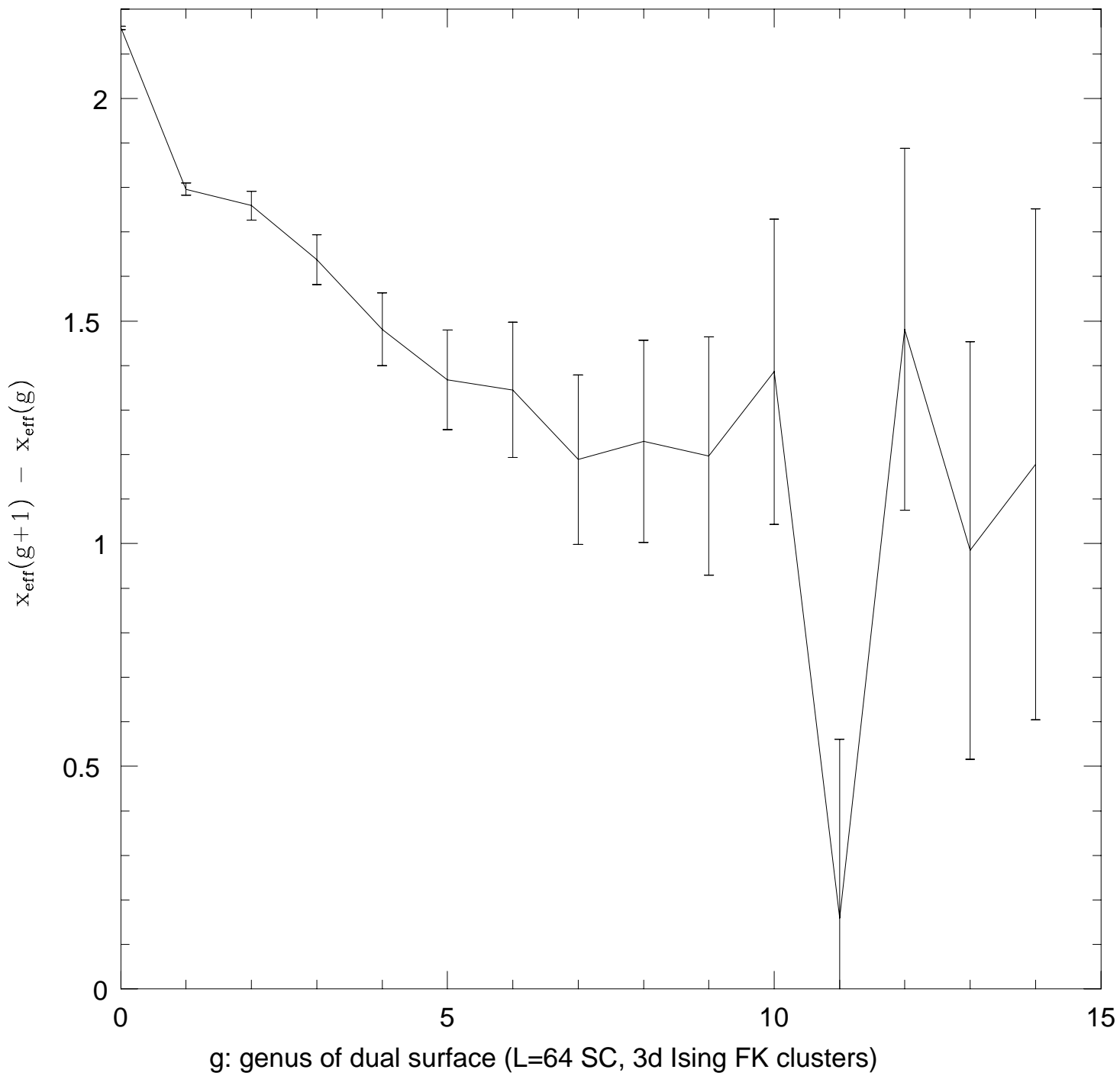


Figure 5.19

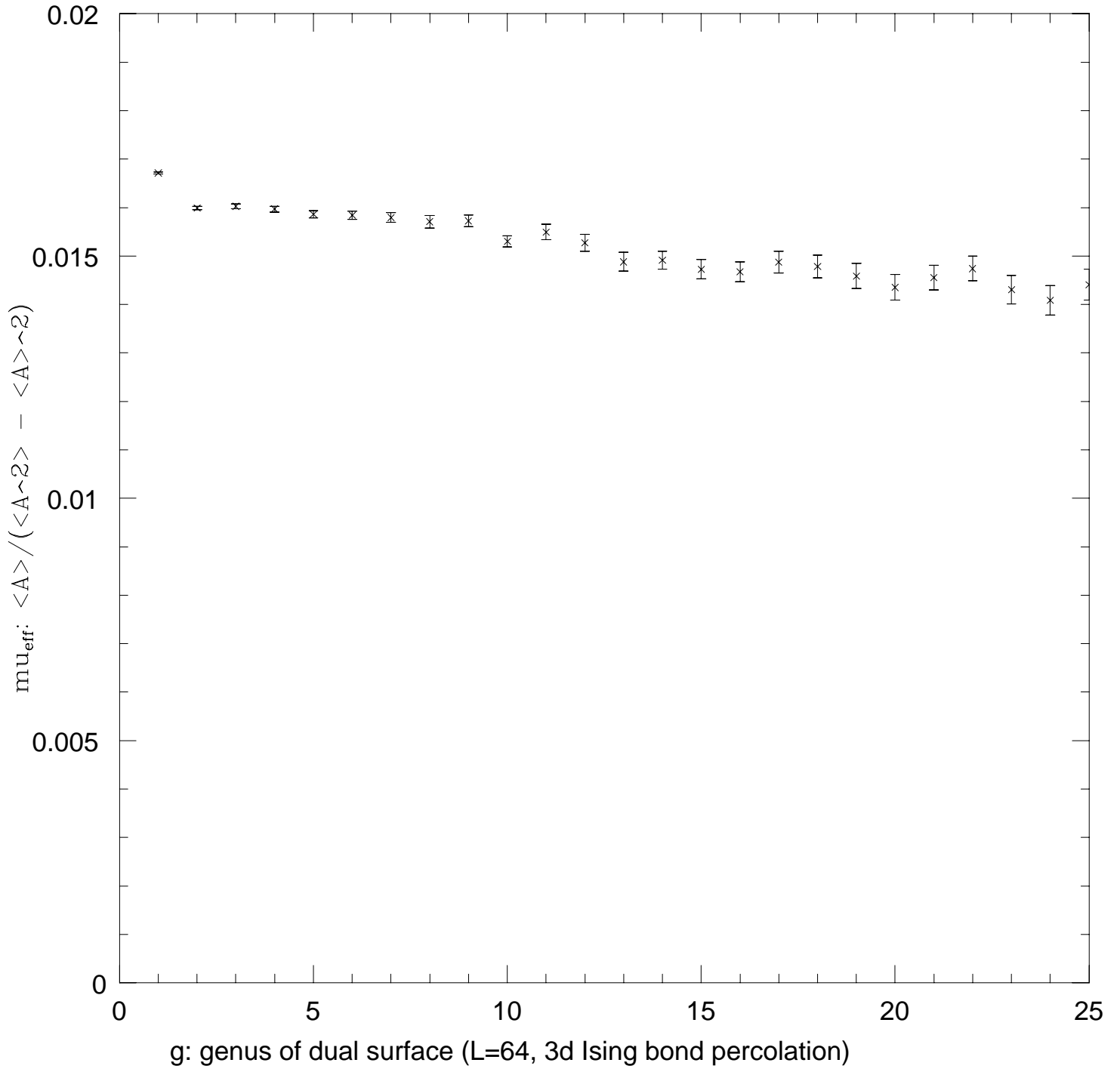


Figure 5.20

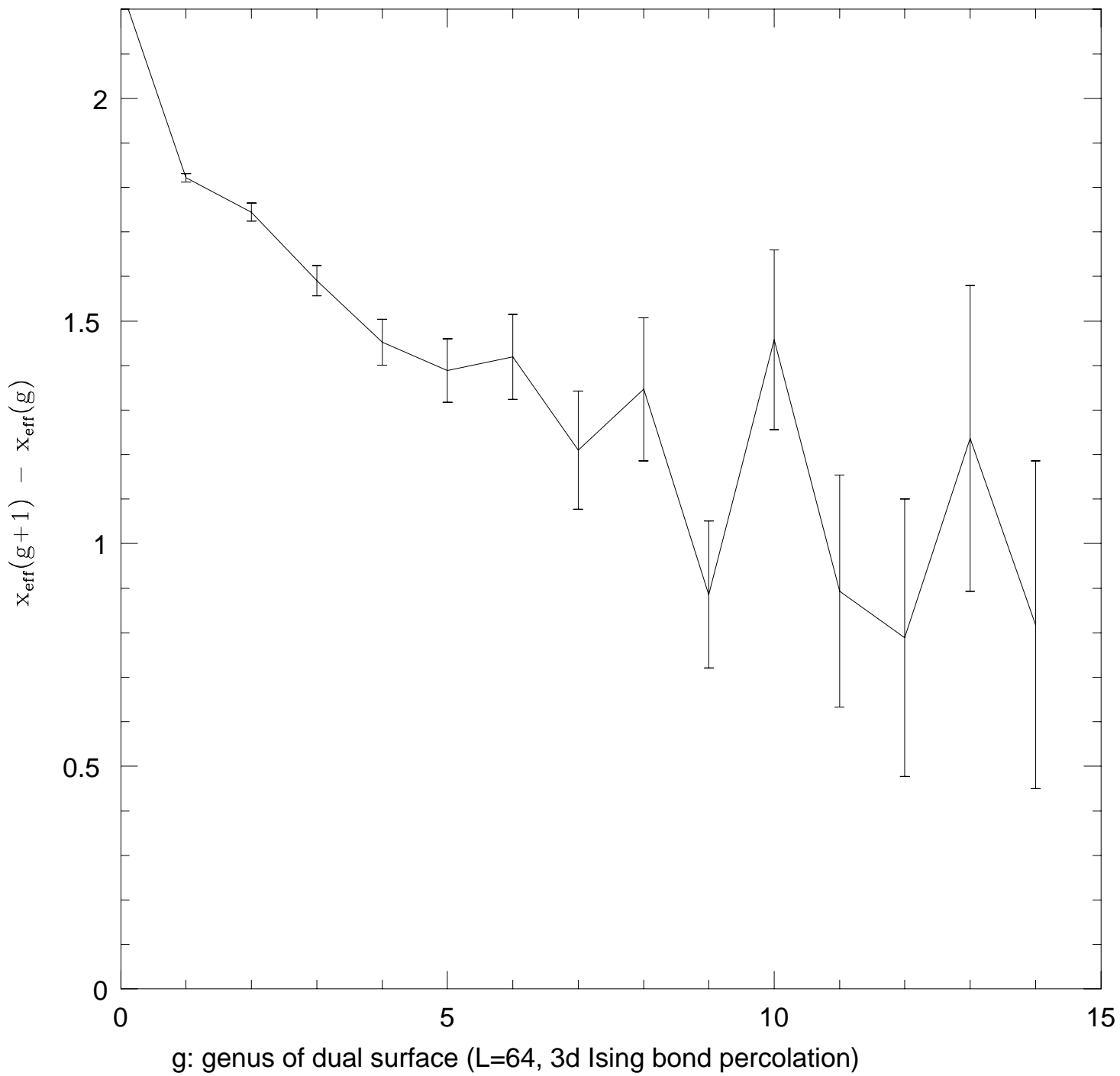


Figure 5.21

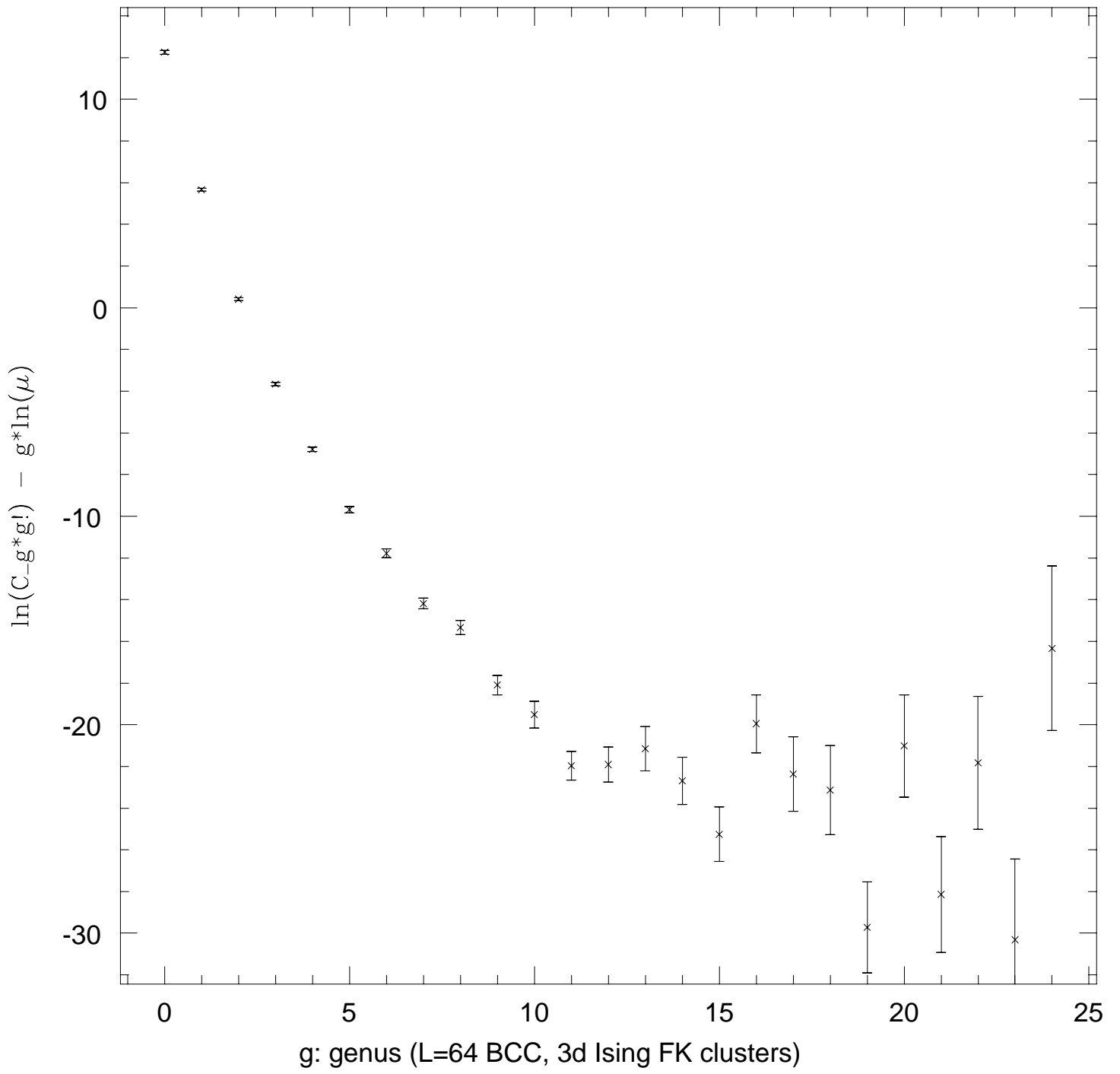


Figure 5.22

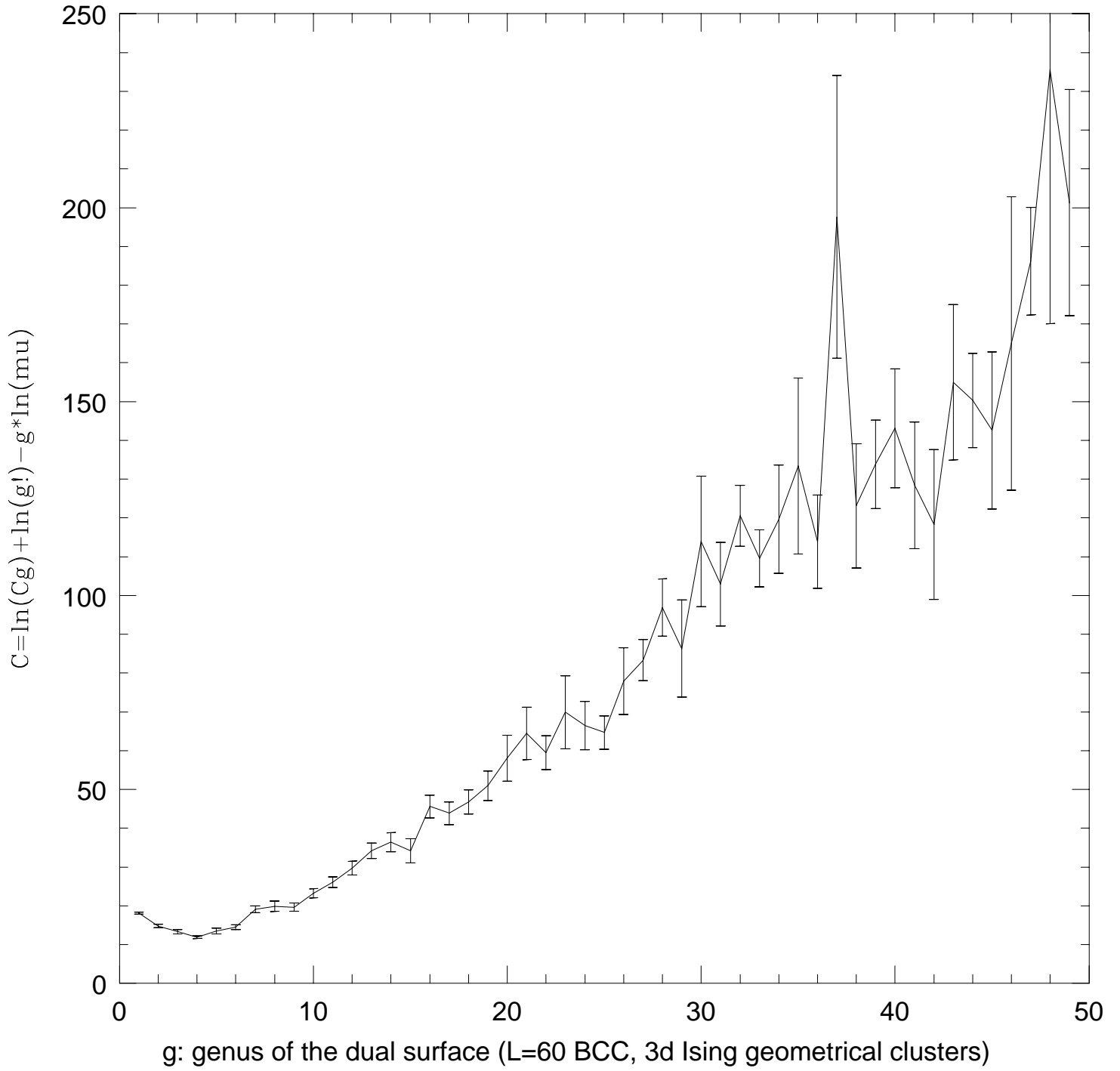


Figure 5.23

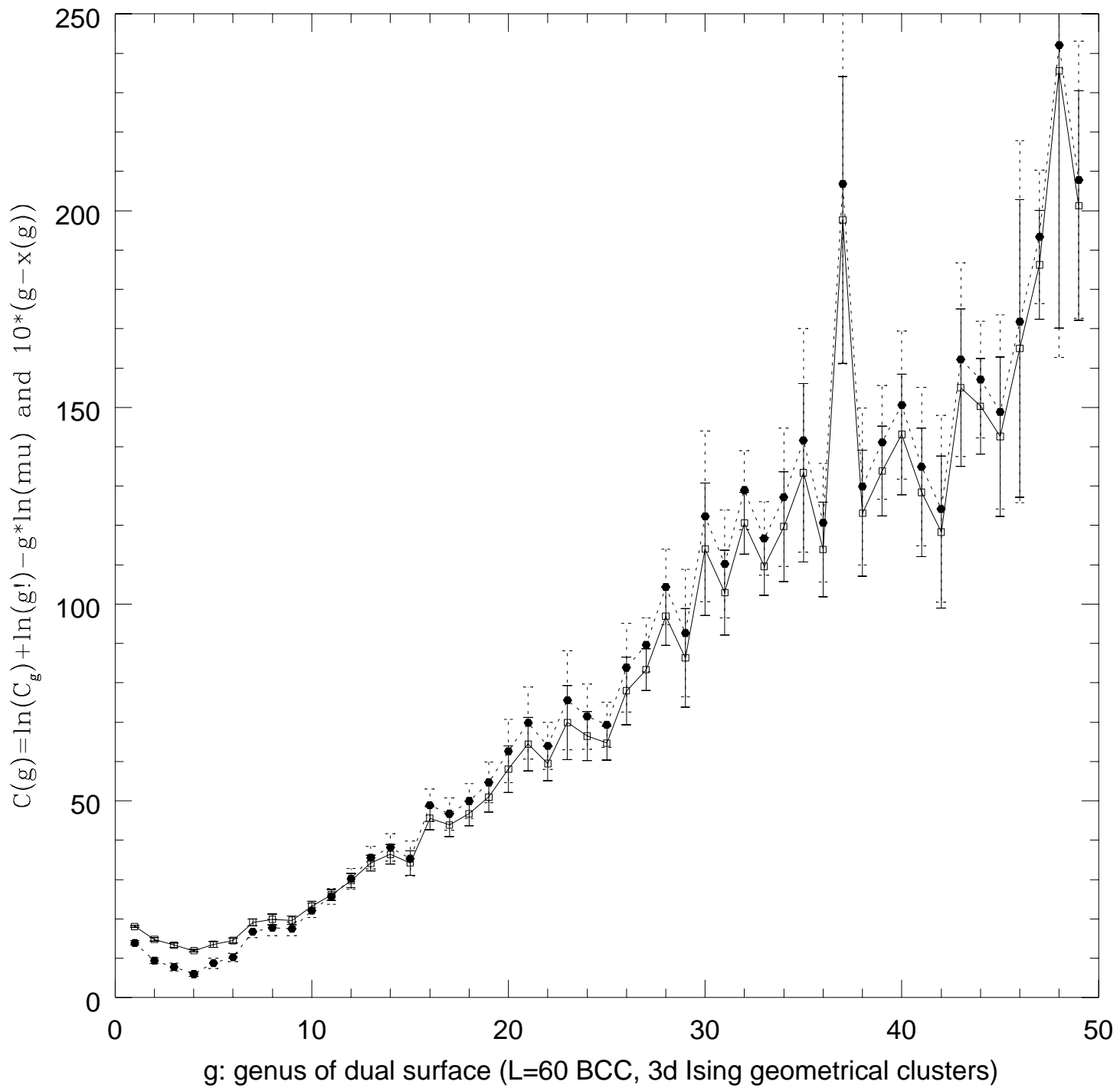


Figure 5.24

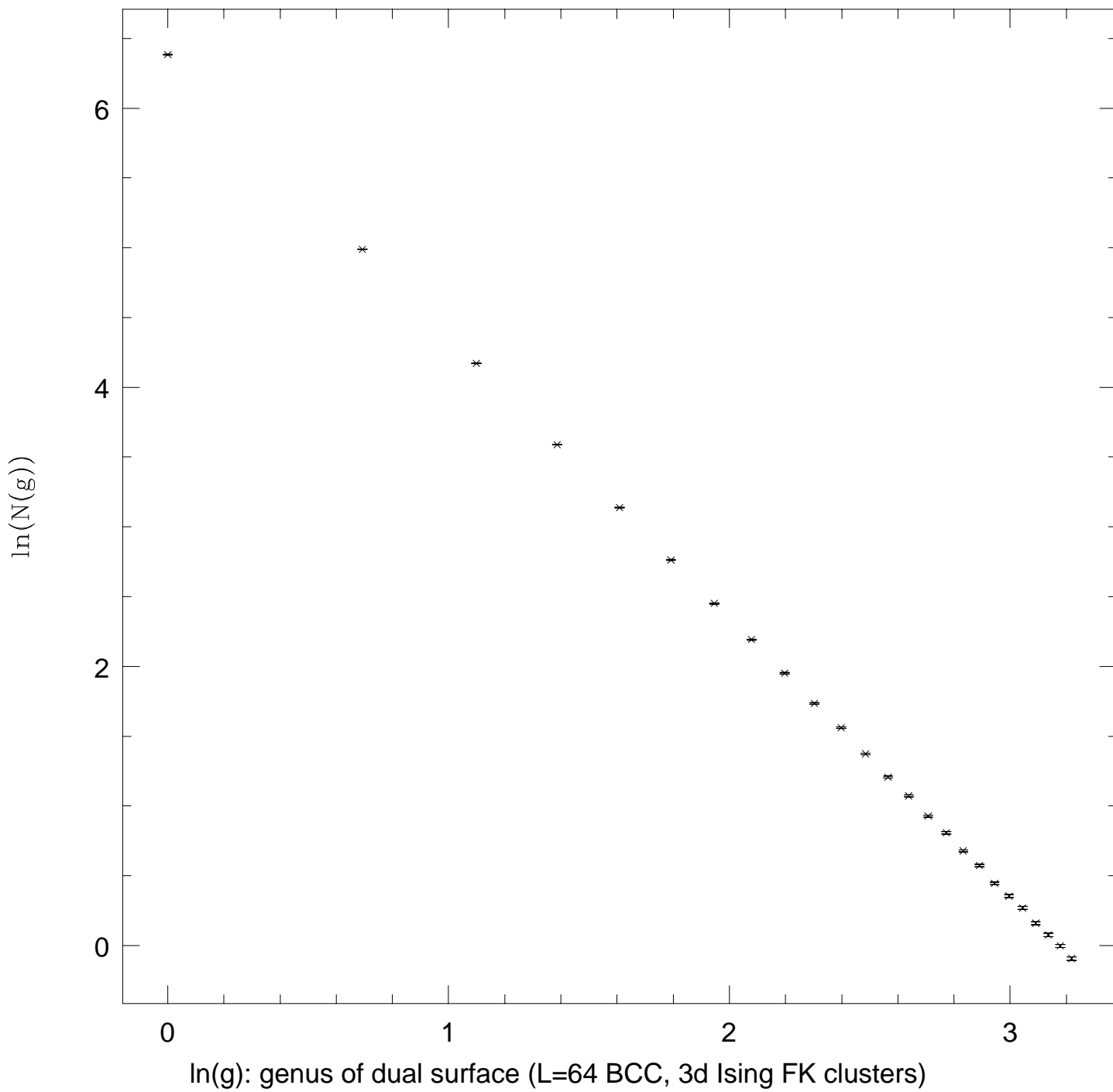


Figure 5.25

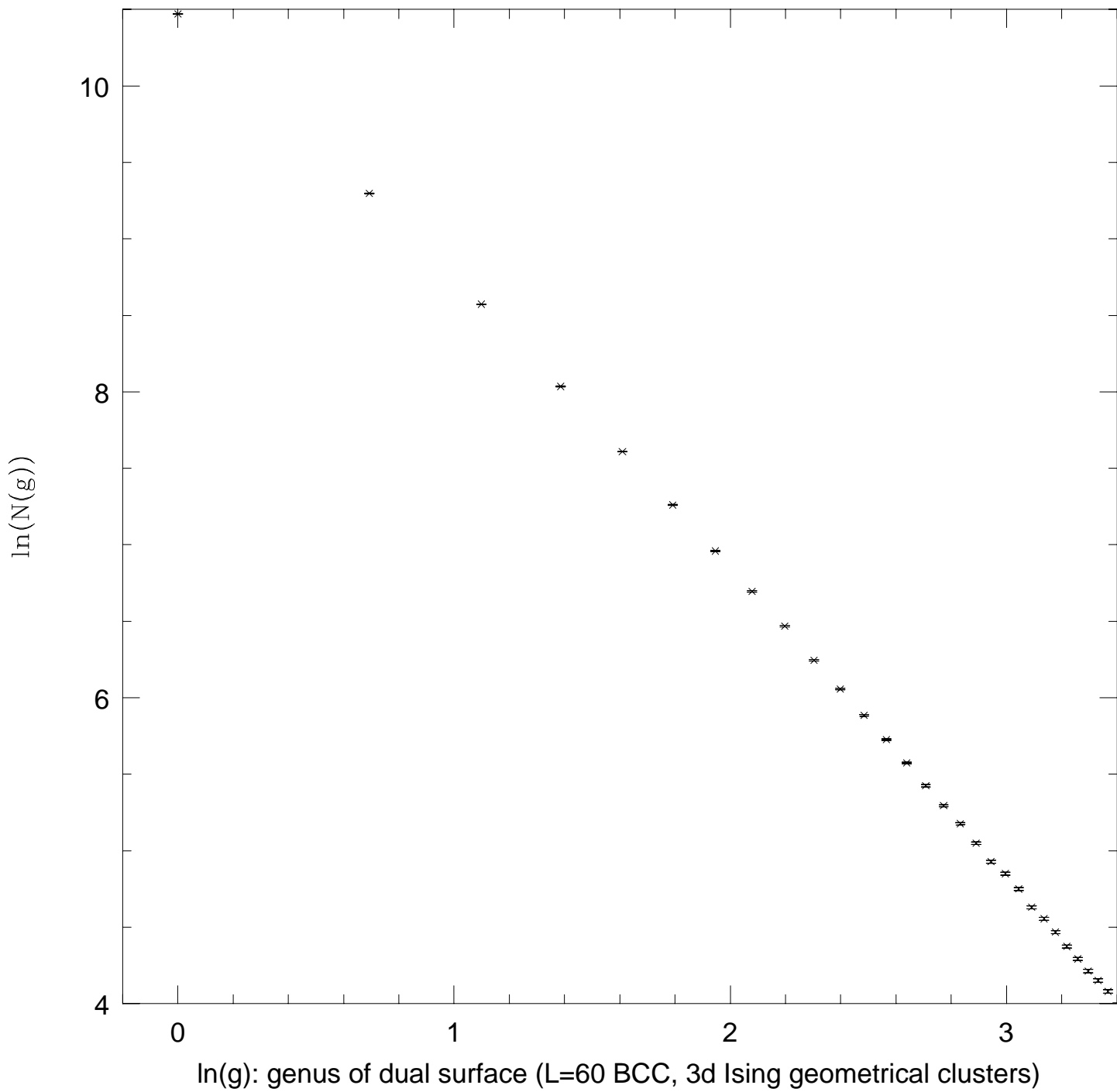


Figure 5.26

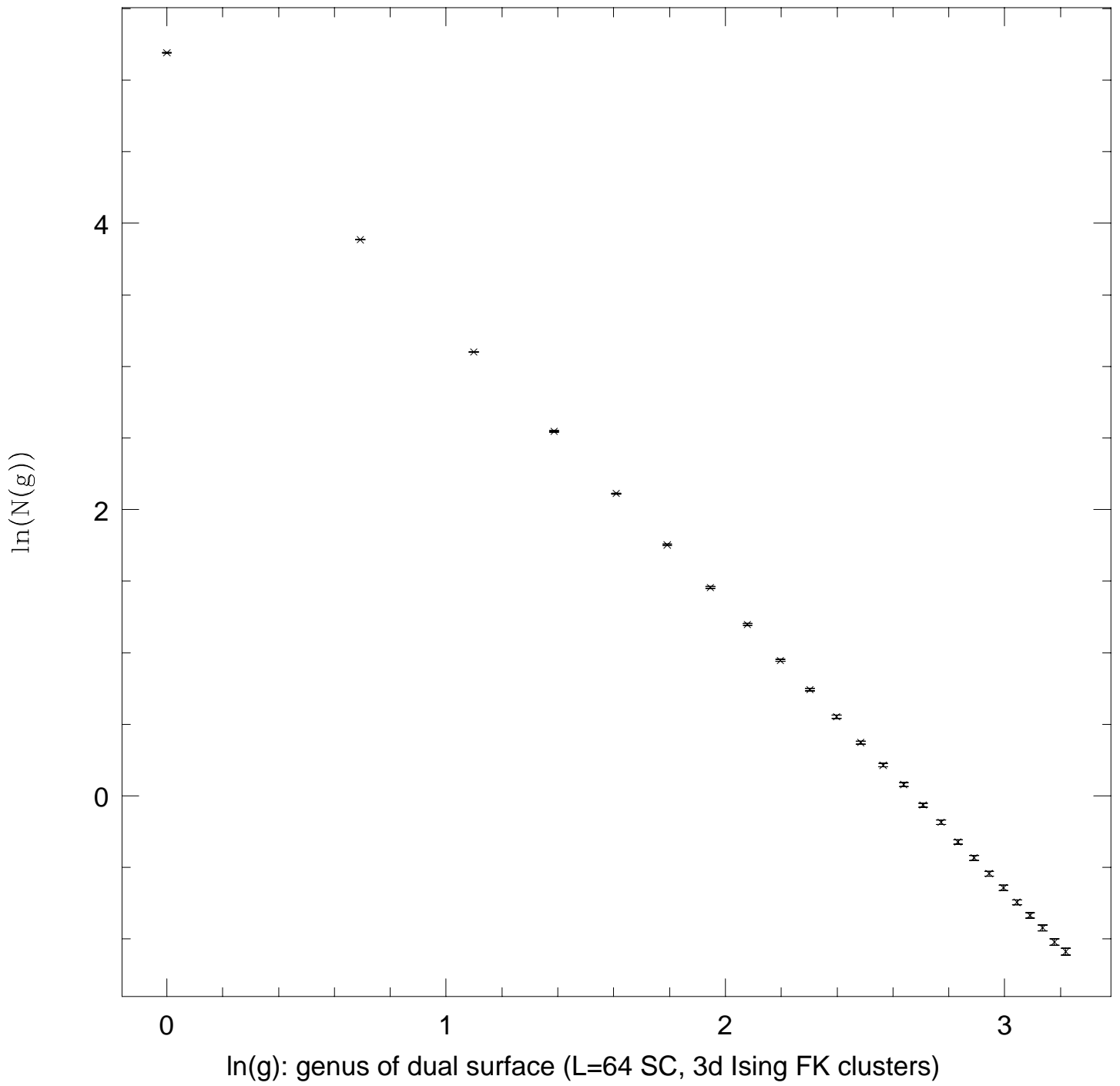


Figure 5.27

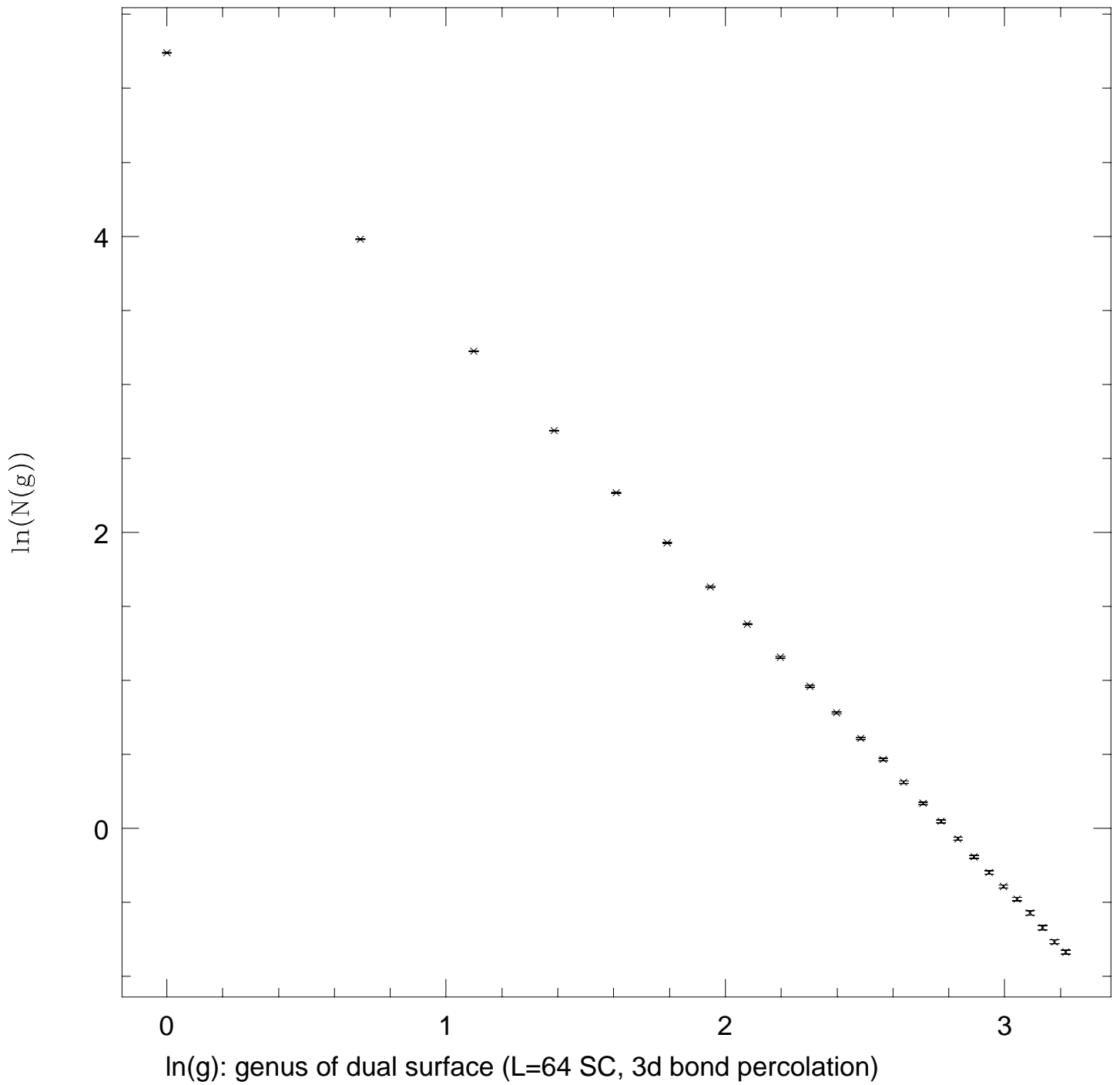


Figure 5.28

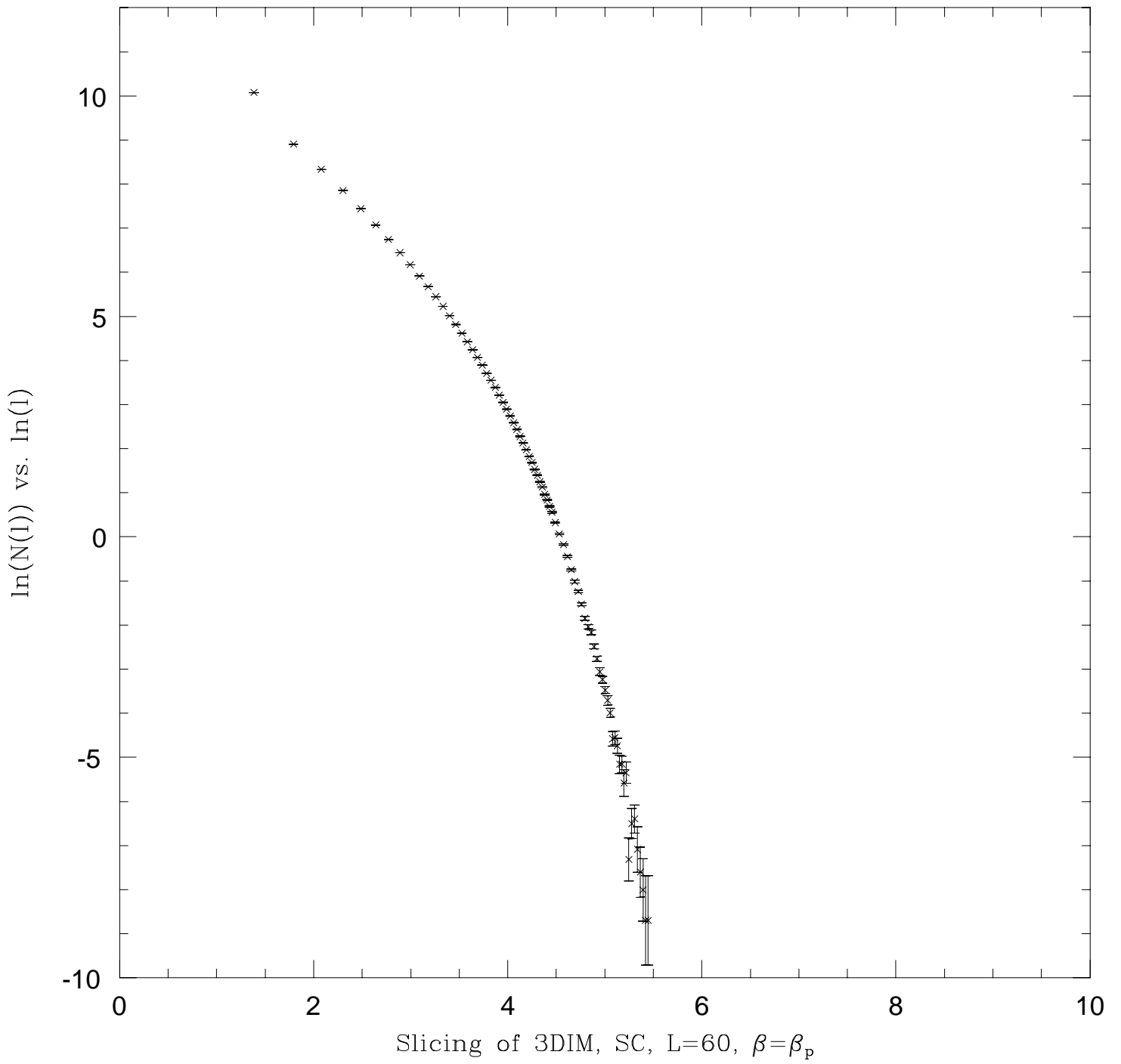
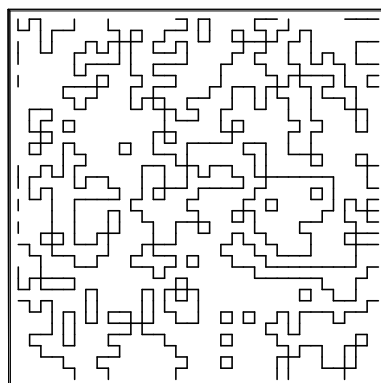
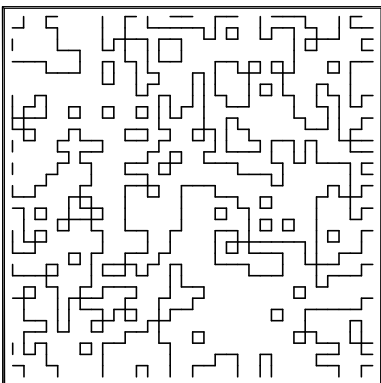
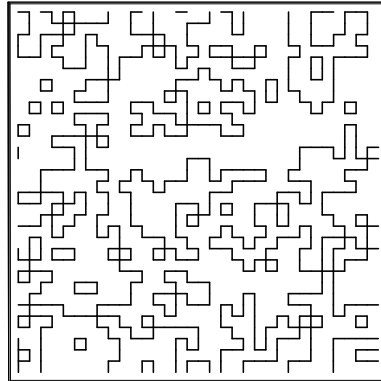
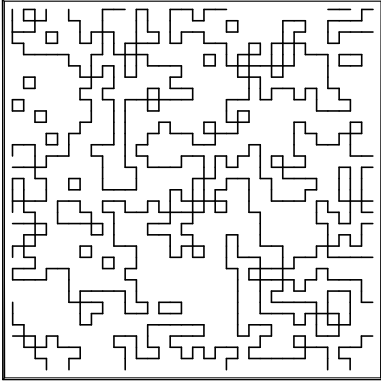


Figure 5.29



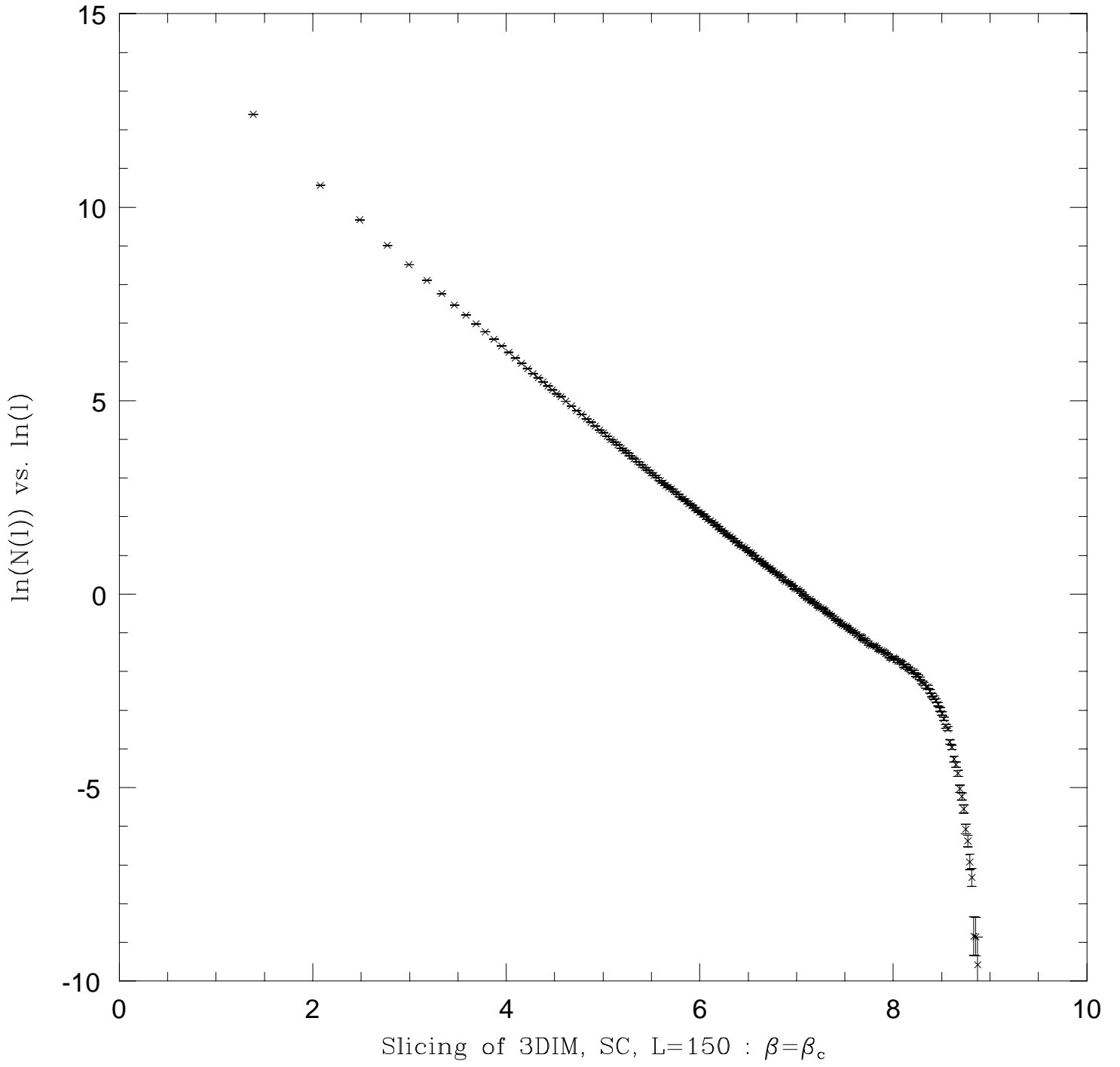


Figure 5.31